

# Exact and Asymptotically Complete Robust Verifications of Neural Networks via Quantum Optimization

Wenxin Li<sup>1†</sup>, Wenchao Liu<sup>1</sup>, Chuan Wang<sup>2\*</sup>, Qi Gao<sup>1</sup>, Yin Ma<sup>1,2</sup>, Hai Wei<sup>1</sup>, Kai Wen<sup>1\*</sup>,

<sup>1</sup>Beijing QBoson Quantum Technology Co., Ltd., Beijing 100015, China

<sup>2</sup>School of Artificial Intelligence, Beijing Normal University, Beijing 100875, China

March 3, 2026

## Abstract

Deep neural networks (DNNs) enable high performance across domains but remain vulnerable to adversarial perturbations, limiting their use in safety-critical settings. Here, we introduce two quantum-optimization-based models for robust verification that reduce the combinatorial burden of certification under bounded input perturbations. For piecewise-linear activations (e.g., ReLU and hardtanh), our first model yields an exact formulation that is sound and complete, enabling precise identification of adversarial examples. For general activations (including sigmoid and tanh), our second model constructs scalable over-approximations via piecewise-constant bounds and is asymptotically complete, with approximation error vanishing as the segmentation is refined. We further integrate Quantum Benders Decomposition with interval arithmetic to accelerate solving, and propose certificate-transfer bounds that relate robustness guarantees of pruned networks to those of the original model. Finally, a layerwise partitioning strategy supports a quantum–classical hybrid workflow by coupling subproblems across depth. Experiments on robustness benchmarks show high certification accuracy, indicating that quantum optimization can serve as a principled primitive for robustness guarantees in neural networks with complex activations.

## Introduction

Neural networks (NNs) have become a cornerstone of modern artificial intelligence, delivering state-of-the-art performance in computer vision [1, 2], natural language processing [3, 4], autonomous systems [5], and scientific discovery [6]. These successes are largely attributed to innovations in deep learning architectures, increased computational power, and the availability of large-scale labeled datasets. Despite their remarkable empirical performance, neural networks remain fundamentally vulnerable to perturbations in their inputs—a property that undermines their reliability in real-world deployments. In safety-critical applications such as autonomous driving, robotic surgery, and automated medical diagnostics, even minor input alterations can lead to severe consequences. For example, as shown in Figure 1, a vision model trained to detect traffic signs may fail to recognize a stop sign if inconspicuous noise or stickers are added to it, triggering potentially dangerous behavior by a self-driving vehicle [7]. Such vulnerabilities highlight a fundamental challenge in the design and deployment of trustworthy AI systems: ensuring robustness to small but adversarial or uncertain changes in input data.

The phenomenon of adversarial vulnerability in neural networks, wherein minor and often imperceptible perturbations to input data can lead to misclassification, was first systematically investigated by Szegedy et al. [8] and subsequently brought to broader attention by Goodfellow et al. through the introduction of the Fast Gradient Sign Method (FGSM) [9]. These so-called adversarial examples demonstrate that modern NNs learn highly non-robust decision boundaries, which can be exploited even by relatively simple perturbation strategies. Addressing these vulnerabilities has emerged as a central challenge in machine learning, catalyzing research in areas such as adversarial training [10], certified defenses [11, 12], and formal verification methods [13, 14]. In particular, formal robustness verification seeks to provide mathematical guarantees that the network’s predictions remain unchanged for all inputs within a specified perturbation region, such as an  $\ell_p$  ball.

Several classical optimization techniques, such as Satisfiability Modulo Theories (SMT) [13], and Branch-and-Bound [15], have been successfully applied to neural network (NN) verification, particularly for networks with ReLU activation functions. The popularity of ReLU stems from its simple structure: it exhibits a binary

<sup>†</sup>Emails: liwx@boseq.com, wangchuan@bnu.edu.cn, wenk@boseq.com

\* Corresponding authors.

behavior where negative inputs yield zero (inactive state) and positive inputs pass through unchanged (active state). This two-state nature simplifies the computational and analytical processes, as each state is either constant or linear. Consequently, verification algorithms based on constraint solving or reachability analysis can leverage this structure to achieve tractable performance. For instance, techniques such as SMT solving (e.g., Reluplex [13]), MILP encoding [14], and reachability-based analysis (e.g., Neurify [16]) can operate effectively on ReLU networks due to their predictable activation patterns and geometrically simpler reachable sets.

While classical verification algorithms are well-suited for networks with ReLU activation functions, they encounter significant challenges when extended to networks with more complex, non-linear activations such as sigmoid or tanh. These functions lack the simple structure of ReLU, making them harder to encode using constraint-based methods. As a result, many approaches rely on intricate approximations or conservative over-approximations, which often lead to a loss in precision. To ensure soundness while coping with these nonlinearities, several verification techniques adopt relaxations or abstractions to improve scalability. However, this typically comes at the cost of completeness; that is, while these methods guarantee that verified properties truly hold (soundness), they may fail to verify properties that are actually valid. In contrast, while methods that attempt to provide both soundness and completeness by precisely computing the reachable set of the network are theoretically rigorous, they are computationally expensive and do not scale well with network depth or size [17], limiting their applicability to small or shallow networks.

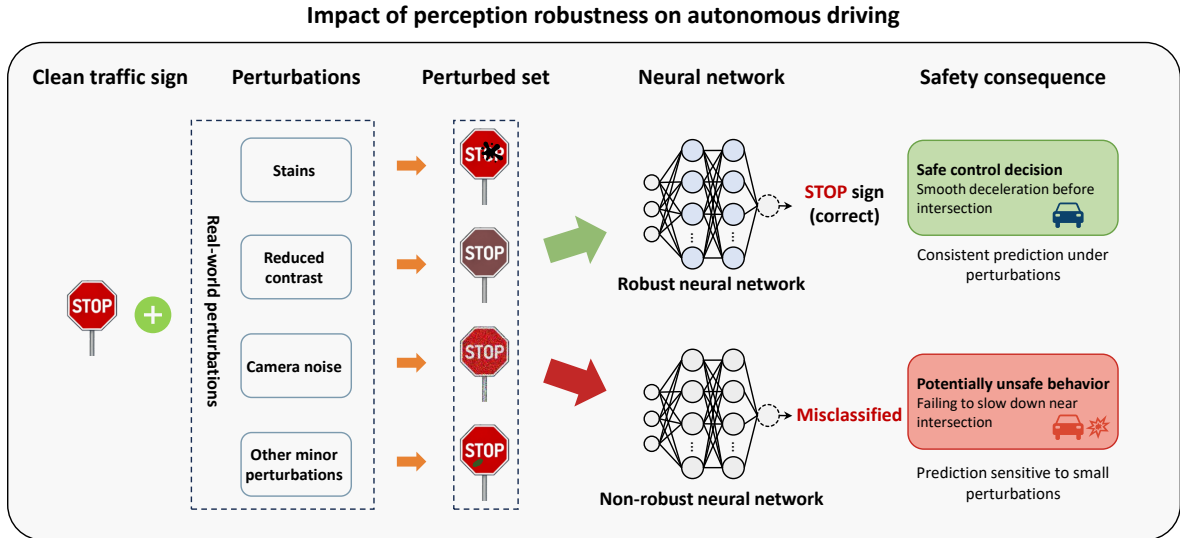


Figure 1: Illustration of adversarial vulnerability in traffic sign recognition. Small, imperceptible perturbations can cause a neural network to misclassify a stop sign, highlighting the need for robust verification.

Verifying the robustness of NNs is, in general, an NP-hard problem [13]. The key challenge lies in determining whether imperceptible input perturbations can lead to incorrect predictions—a task that necessitates exploring a high-dimensional, non-convex optimization landscape. As NN architectures grow increasingly complex, classical verification methods encounter significant computational bottlenecks. Recent advances in quantum hardware, including IBM Quantum’s superconducting processors, Google’s demonstration of quantum supremacy [18], and D-Wave’s recent quantum-annealing milestone with the Advantage2 system [19], have positioned quantum computing as a promising avenue for tackling problems that are formally intractable for classical systems. Concurrently, the emergence of quantum machine learning (QML) has opened new directions for incorporating specialized hardware into machine learning workflows [20, 21, 22, 23]. In the specific domain of NN robustness verification, hybrid quantum-classical approaches based on Ising-model optimization and quantum annealing have garnered increasing interest. Notably, Franco et al. [24] propose a hybrid certification algorithm that reformulates the verification problem as a quadratic unconstrained binary optimization (QUBO) task, enabling the generation of provable robustness certificates on quantum hardware. By leveraging the mapping to the Ising model, such techniques offer a potential pathway to mitigating the combinatorial explosion inherent in neural network verification.

Building upon the potential of quantum computing in NN robustness verification, our work proposes two novel models that integrate quantum optimization techniques to tackle the verification challenges posed by general classes of activation functions. The first model focuses on networks with arbitrary piecewise linear activation

functions. For this class, we provide a verification framework that is both sound and complete, ensuring exactness while addressing the scalability limitations of existing methods. By encoding the verification problem into a quantum-amenable optimization formulation, this model leverages the structure of piecewise linearity to enable efficient yet rigorous certification. The second model extends to networks with arbitrary (possibly non-linear and non-piecewise-linear) activation functions. Drawing inspiration from the structure and formulation of the first model, we propose a method for computing both upper and lower bounds on the output reachable set. While this model does not guarantee completeness, it is sound and introduces a novel theoretical property, which we term asymptotic completeness: as the number of discretization variables increases, the approximation error can asymptotically vanish, approaching the true reachable set. Together, these two models constitute a meaningful step forward at the intersection of quantum optimization and neural network verification. By introducing asymptotic completeness for general activation functions, our work broadens the scope of provable robustness analysis and demonstrates the potential for quantum computing to achieve more scalable and expressive guarantees in NN verification.

The following table summarizes these contributions, highlighting the characteristics and supported activation functions.

Model	Activation Functions	Sound	Complete
Model 1	Piecewise Linear	✓	✓
Model 2	Arbitrary Nonlinear	✓	Asymptotic Complete

Table 1: Summary of the two models in this paper

## Results

Deep neural networks (DNNs) are susceptible to adversarial perturbations, which are small changes to inputs that can lead to incorrect predictions. Robustness verification seeks to formally guarantee that a neural network’s predictions remain consistent under bounded perturbations. Given a trained neural network  $f : \mathbb{R}^d \rightarrow \mathbb{R}^K$ , where  $d$  is the input dimension and  $K$  is the number of output classes, let  $\mathbf{x}_0 \in \mathbb{R}^d$  be a nominal input with true label  $y_{\text{true}} = \arg \max_k f_k(\mathbf{x}_0)$ . For a perturbation budget  $\epsilon > 0$ , the  $\ell_\infty$ -ball around  $\mathbf{x}_0$  is defined as:

$$\mathcal{B}_\infty(\mathbf{x}_0, \epsilon) := \{\mathbf{x} \in \mathbb{R}^d \mid \|\mathbf{x} - \mathbf{x}_0\|_\infty \leq \epsilon\}.$$

The network is *locally robust* at  $\mathbf{x}_0$  if:

$$\forall \mathbf{x} \in \mathcal{B}_\infty(\mathbf{x}_0, \epsilon), \quad \arg \max_k f_k(\mathbf{x}) = y_{\text{true}}.$$

Equivalently, robustness is violated if there exists an adversarial example  $\mathbf{x} \in \mathcal{B}_\infty(\mathbf{x}_0, \epsilon)$  such that:

$$f_{y_p}(\mathbf{x}) \geq f_{y_{\text{true}}}(\mathbf{x}), \quad \text{for some } y_p \neq y_{\text{true}}.$$

The verification task is to determine whether such an adversarial example exists, which can be formulated as an optimization problem over the neural network’s output within the perturbation ball. The overall workflow of our proposed framework is illustrated in Figure 2.

Let  $f : \mathbb{R}^d \rightarrow \mathbb{R}^K$  be the original classifier and  $g$  its pruned counterpart. For a labeled input  $(x, y)$ , define the logit margin

$$m_f(x) = f_y(x) - \max_{k \neq y} f_k(x), \quad \Phi_f(x; \epsilon) = \inf_{\|\delta\|_p \leq \epsilon} m_f(x + \delta),$$

and certified accuracy  $\text{CA}_f(\epsilon) = \frac{1}{|S|} \sum_{(x,y) \in S} \mathbf{1}\{\Phi_f(x; \epsilon) > 0\}$ .

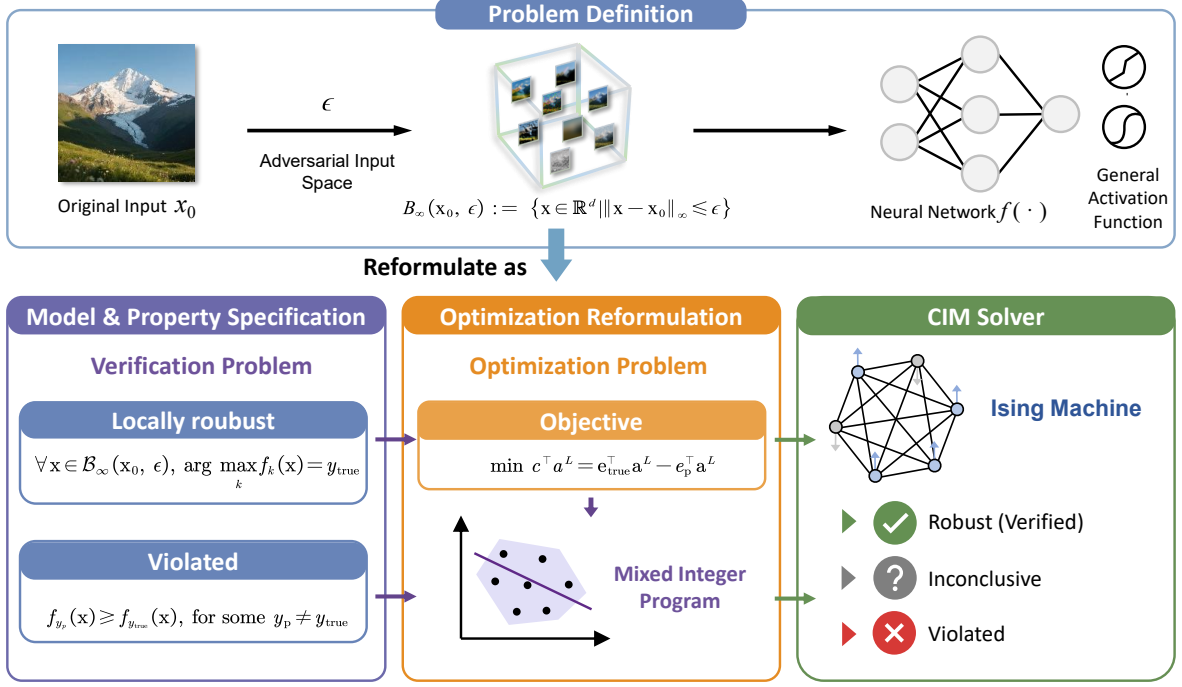


Figure 2: Overview of the proposed quantum-amenable robustness verification workflow. The framework formulates the verification problem for an activation function as an optimization task, and solves it using an Ising solver.

## Model for Piecewise Activation Linear function

Consider a neural network comprising  $L$  layers, with the input  $\mathbf{x} \in \mathbb{R}^{n_0}$  subject to perturbations within an  $\ell_\infty$ -ball of radius  $\epsilon$  centered at a nominal point  $\mathbf{x}_0$ . The goal is to determine the tightest bound on the output  $y = a_0^L$ , expressed through the optimization problem:

$$\min \mathbf{c}^\top \mathbf{a}^L = \mathbf{e}_{\text{true}}^\top \mathbf{a}^L - \mathbf{e}_p^\top \mathbf{a}^L, \quad (1)$$

where  $\mathbf{a}^L \in \mathbb{R}^{n_L}$  denotes the final layer activations, with  $n_L = 1$  for the single output  $a_0^L$ , and  $\mathbf{c} = \mathbf{e}_{\text{true}} - \mathbf{e}_p \in \mathbb{R}^{n_L}$  incorporates indicator vectors  $\mathbf{e}_{\text{true}}$  and  $\mathbf{e}_p$  for the target and perturbed outputs.

Let  $\mathbf{y} = [\mathbf{x}^\top (\mathbf{a}^1)^\top (\mathbf{z}^1)^\top (\mathbf{u}^1)^\top \dots (\mathbf{a}^L)^\top (\mathbf{z}^L)^\top (\mathbf{u}^L)^\top]^\top \in \mathbb{R}^{n_0 + \sum_{l=1}^L (n_l + n_l + n_l \cdot n)}$ , with  $\mathbf{u}^l = [u_{j,i}^l] \in \mathbb{R}^{n_l \cdot n}$  as auxiliary variables. The formulation relies on constraints that trace the network's behavior, leveraging binary variables  $\beta = \{\beta_{z_j^l}^{(i)}\}_{l,j,i}$  to pinpoint segments  $[M_{i-1}, M_i]$  corresponding to pre-activation values  $z_j^l$ .

To enhance clarity and computational tractability, we articulate these constraints in matrix form:

1. **Input Constraints:** The input  $\mathbf{x} = \mathbf{a}_x^0$  is restricted to an  $\ell_\infty$ -ball:

$$\begin{bmatrix} \mathbf{I}_{n_0} \\ -\mathbf{I}_{n_0} \end{bmatrix} \mathbf{x} \leq \begin{bmatrix} \mathbf{x}_0 + \epsilon \mathbf{1} \\ -(\mathbf{x}_0 - \epsilon \mathbf{1}) \end{bmatrix} = \mathbf{d}_{\text{input}}. \quad (2)$$

We now shift our focus to encapsulate these restrictions within a unified framework using the complete vector  $\mathbf{y}$ ,

$$\mathbf{C}_{\text{input}} \mathbf{y} \leq \mathbf{d}_{\text{input}},$$

where

$$\mathbf{C}_{\text{input}} = [\mathbf{I}_{n_0} \quad \mathbf{0} \quad \dots \quad \mathbf{0}] \in \mathbb{R}^{2n_0 \times (n_0 + \sum_{l=1}^L (n_l + n_l + n_l \cdot n))}, \quad (3)$$

2. **Pre-activation Bounds:** For each layer  $l = 1, \dots, L$  and neuron  $j = 1, \dots, n_l$ , the pre-activation is defined as:

$$z_j^l - \sum_{k=1}^{n_{l-1}} w_{jk}^l a_k^{l-1} = b_j^l, \quad (4)$$

where  $w_{jk}^l$  are weights and  $b_j^l$  are biases. The weight matrix  $\mathbf{W}^l \in \mathbb{R}^{n_l \times n_{l-1}}$  has  $(\mathbf{W}^l)_{jk} = w_{jk}^l$ . In matrix notation:

$$\mathbf{z}^l - \mathbf{W}^l \mathbf{a}^{l-1} = \mathbf{b}^l,$$

with  $\mathbf{b}^l = [b_1^l, \dots, b_{n_l}^l]^\top \in \mathbb{R}^{n_l}$ . We proceed to integrate these into a cohesive matrix representation based on the full vector  $\mathbf{y}$ ,

$$\mathbf{A}_{\text{pre}}^l \mathbf{y} = \mathbf{b}^l,$$

where the layer-specific matrix is

$$\mathbf{A}_{\text{pre}}^l = [\mathbf{0} \quad \dots \quad -\mathbf{W}^l \quad \mathbf{I}_{n_l} \quad \mathbf{0} \quad \dots] \in \mathbb{R}^{n_l \times (n_0 + \sum_{i=1}^L (n_i + n_i + n_i \cdot n))},$$

featuring  $\mathbf{I}_{n_l}$  for  $\mathbf{z}^l$  and  $-\mathbf{W}^l$  for  $\mathbf{a}^{l-1}$ , with zeros elsewhere. This constraint traces the linear flow of pre-activations.

**3. Activation Bounds:** The activation values are expressed as:

$$a_j^l = \sum_{i=1}^n \beta_{z_j^l}^{(i)} (\alpha_i z_j^l + \gamma_i), \quad (5)$$

linearized with auxiliary variables  $u_{j,i}^l = \beta_{z_j^l}^{(i)} z_j^l$ . The binary matrix  $\mathbf{B}_\beta^l \in \mathbb{R}^{n_l \times n}$  has the  $j$ -th row  $\beta_{z_j^l}^\top = [\beta_{z_j^l}^{(1)}, \dots, \beta_{z_j^l}^{(n)}]$ . The reformulated expression is:

$$a_j^l = \sum_{i=1}^n (\alpha_i u_{j,i}^l + \gamma_i \beta_{z_j^l}^{(i)}).$$

In matrix terms:

$$\mathbf{a}^l = \mathbf{A}_{\text{act},1}^l \mathbf{u}^l + \mathbf{A}_{\text{act},2}^l \boldsymbol{\beta}^l,$$

where  $\boldsymbol{\beta}^l = [\beta_{z_1^l}, \dots, \beta_{z_{n_l}^l}]^\top \in \mathbb{R}^{n_l \cdot n}$ , and

$$\mathbf{A}_{\text{act},1}^l = \text{diag}(\alpha_1, \dots, \alpha_n) \otimes \mathbf{I}_{n_l}, \quad \mathbf{A}_{\text{act},2}^l = \mathbf{I}_{n_l} \otimes \boldsymbol{\gamma},$$

with  $\boldsymbol{\gamma} = [\gamma_1, \dots, \gamma_n]^\top$ . Extracting  $\boldsymbol{\beta}_{\text{slice}}^l$  using a selection matrix  $\mathbf{S}^l \in \mathbb{R}^{n_l \cdot n \times L \cdot n_L \cdot n}$ , where  $\mathbf{S}^l \boldsymbol{\beta} = \boldsymbol{\beta}_{\text{slice}}^l$ , we have

$$\mathbf{A}_{\text{act}}^l \mathbf{y} = \mathbf{A}_{\text{act},2}^l \mathbf{S}^l \boldsymbol{\beta},$$

where

$$\mathbf{A}_{\text{act}}^l = [\mathbf{0} \quad \dots \quad \mathbf{I}_{n_l} \quad \mathbf{0} \quad -\mathbf{A}_{\text{act},1}^l \quad \mathbf{0} \quad \dots] \in \mathbb{R}^{n_l \times (n_0 + \sum_{i=1}^L (n_i + n_i + n_i \cdot n))},$$

aligning  $\mathbf{I}_{n_l}$  with  $\mathbf{a}^l$ ,  $-\mathbf{A}_{\text{act},1}^l$  with  $\mathbf{u}^l$ . This captures the segmented linear nature of activations based on chosen intervals.

**4. Piecewise Linear Constraints:** Pre-activation values are confined to segments  $[M_{i-1}, M_i]$ :

$$z_j^l \geq \sum_{i=1}^n M_{i-1} \beta_{z_j^l}^{(i)}, \quad z_j^l \leq \sum_{i=1}^n M_i \beta_{z_j^l}^{(i)}, \quad (6)$$

using segment boundaries  $\mathbf{M}_- = [M_0, \dots, M_{n-1}]^\top \in \mathbb{R}^n$  and  $\mathbf{M}_+ = [M_1, \dots, M_n]^\top \in \mathbb{R}^n$ . Using the Kronecker product:

- $\mathbf{A}_{\text{lower}}^l = \mathbf{I}_{n_l} \otimes \mathbf{M}_-^\top \in \mathbb{R}^{n_l \times (n_l \cdot n)}$ ,
- $\mathbf{A}_{\text{upper}}^l = \mathbf{I}_{n_l} \otimes \mathbf{M}_+^\top \in \mathbb{R}^{n_l \times (n_l \cdot n)}$ .

Then we can compile these into a consolidated matrix inequality across the full  $\mathbf{y}$ ,

$$\mathbf{C}_{\text{pwl}}^l \mathbf{y} \leq \mathbf{d}_{\text{pwl}}^l \boldsymbol{\beta},$$

where

$$\mathbf{C}_{\text{pwl}}^l = \begin{bmatrix} \mathbf{0} & \dots & \mathbf{0} & -\mathbf{I}_{n_l} & \mathbf{0} & \mathbf{0} & \dots \\ \mathbf{0} & \dots & \mathbf{0} & \mathbf{I}_{n_l} & \mathbf{0} & \mathbf{0} & \dots \end{bmatrix} \in \mathbb{R}^{2n_l \times (n_0 + \sum_{i=1}^L (n_i + n_i + n_i \cdot n))}, \quad (7)$$

$$\mathbf{d}_{\text{pwl}}^l = \begin{bmatrix} -\mathbf{A}_{\text{lower}}^l \mathbf{S}^l \\ \mathbf{A}_{\text{upper}}^l \mathbf{S}^l \end{bmatrix}, \quad (8)$$

with  $\mathbf{I}_{n_l}$  corresponding to  $\mathbf{z}^l$ , zeros elsewhere. These ensure pre-activations adhere to the selected segment boundaries, upholding the piecewise framework.

5. **Linearization Constraints:** The auxiliary variables  $u_{j,i}^l = \beta_{z_j^l}^{(i)}$  are governed by the big-M method:

$$u_{j,i}^l \leq \bar{M}\beta_{z_j^l}^{(i)}, \quad (9)$$

$$u_{j,i}^l \geq \underline{M}\beta_{z_j^l}^{(i)}, \quad (10)$$

$$u_{j,i}^l \leq z_j^l - \underline{M}(1 - \beta_{z_j^l}^{(i)}), \quad (11)$$

$$u_{j,i}^l \geq z_j^l - \bar{M}(1 - \beta_{z_j^l}^{(i)}), \quad (12)$$

for all  $l, j, i$ . In matrix terms, with  $\mathbf{u}^l = [u_{1,1}^l, \dots, u_{n_l, n}^l]^\top \in \mathbb{R}^{n_l \cdot n}$ ,  $\mathbf{z}^l \in \mathbb{R}^{n_l}$ , and  $\beta^l \in \mathbb{R}^{n_l \cdot n}$ . This constraint can be formulated as

$$\mathbf{A}^l \mathbf{y} + \mathbf{B}^l \beta \geq \mathbf{c}^l = \begin{bmatrix} \mathbf{0} \\ \mathbf{0} \\ -\underline{M}\mathbf{1}_{n_l \cdot n} \\ -\bar{M}\mathbf{1}_{n_l \cdot n} \end{bmatrix},$$

where  $\mathbf{A}^l \in \mathbb{R}^{4n_l \cdot n \times (n_0 + \sum_{l=1}^L (2n_l + n_l \cdot n))}$  has non-zero blocks at  $\mathbf{u}^l$  and  $\mathbf{z}^l$ ,

$$\mathbf{A}^l = \begin{bmatrix} \mathbf{0} & \cdots & \mathbf{0} & -\mathbf{I}_{n_l \cdot n} & \mathbf{0} & \mathbf{0} & \cdots & \mathbf{0} \\ \mathbf{0} & \cdots & \mathbf{0} & \mathbf{I}_{n_l \cdot n} & \mathbf{0} & \mathbf{0} & \cdots & \mathbf{0} \\ \mathbf{0} & \cdots & \mathbf{0} & -\mathbf{I}_{n_l \cdot n} & \mathbf{I}_{n_l} & \mathbf{0} & \cdots & \mathbf{0} \\ \mathbf{0} & \cdots & \mathbf{0} & \mathbf{I}_{n_l \cdot n} & -\mathbf{I}_{n_l} & \mathbf{0} & \cdots & \mathbf{0} \end{bmatrix},$$

here  $-\mathbf{I}_{n_l \cdot n}$  and  $\pm\mathbf{I}_{n_l}$  are at the  $\mathbf{u}^l$  and  $\mathbf{z}^l$  positions, and

$$\mathbf{B}^l = \begin{bmatrix} \bar{M}\mathbf{S}^l \\ -\underline{M}\mathbf{S}^l \\ \underline{M}\mathbf{S}^l \\ -\bar{M}\mathbf{S}^l \end{bmatrix}.$$

This linearization transforms the nonlinear product into a solvable form.

6. **Binary Constraints:** Segment selection is enforced by:

$$\sum_{i=1}^n \beta_{z_j^l}^{(i)} = 1, \quad \beta_{z_j^l}^{(i)} \in \{0, 1\}, \quad (13)$$

With  $\mathbf{A}_{\text{bin}}^l = \text{diag}(\mathbf{1}_n^\top, \dots, \mathbf{1}_n^\top)$ , we have

$$\mathbf{A}_{\text{bin}}^l \beta^l = \mathbf{1}_{n_l},$$

and consequently

$$\mathbf{A}_{\text{bin}}^l \mathbf{S}^l \beta = \mathbf{1}_{n_l}.$$

## Model for Arbitrary Non-linear Activation Functions

Deep neural networks (DNNs) employing arbitrary activation functions, such as sigmoid, tanh, or other non-piecewise-linear functions, pose significant challenges for robustness verification due to their inherent nonlinearity. Traditional methods, which excel with piecewise linear activations like ReLU, often fail to generalize effectively to these cases, leaving a gap in verifying legacy models or networks designed for specific applications. To address this, we propose Model 2, a novel framework that leverages piecewise constant bounds to approximate and verify the robustness of DNNs with arbitrary activation functions. This model is inspired by the conceptual framework illustrated in Figure 3, which depicts a sigmoid curve bounded by upper and lower piecewise constant functions, providing a practical approach to handle complex nonlinearities.

Consider a neural network with  $L$  layers, where the input  $\mathbf{x} \in \mathbb{R}^{n_0}$  is perturbed within an  $\ell_\infty$ -ball of radius  $\varepsilon$  around a nominal point  $\mathbf{x}_0$ . Define the vector  $\mathbf{y} = [\mathbf{x}, \mathbf{a}^1, \bar{\mathbf{a}}^1, \underline{\mathbf{z}}^1, \bar{\mathbf{z}}^1, \dots, \mathbf{a}^L, \bar{\mathbf{a}}^L, \underline{\mathbf{z}}^L, \bar{\mathbf{z}}^L]^\top \in \mathbb{R}^{n_0 + 4 \sum_{l=1}^L n_l}$ . The objective is to compute the tightest bounds on the output  $y = a_0^L$ , formulated as:

$$\min \quad \mathbf{c}^\top \mathbf{y}^L = \mathbf{e}_{\text{true}}^\top \mathbf{a}^L - \mathbf{e}_{\text{p}}^\top \bar{\mathbf{a}}^L, \quad (14)$$

where  $\mathbf{y}^L = [(\underline{\mathbf{a}}^L)^\top, (\bar{\mathbf{a}}^L)^\top]^\top \in \mathbb{R}^{2n_L}$ ,  $\underline{\mathbf{a}}^L, \bar{\mathbf{a}}^L \in \mathbb{R}^{n_L}$  are the lower and upper bounds of the final layer activations, and  $\mathbf{c} = [\mathbf{e}_{\text{true}}^\top, -\mathbf{e}_p^\top]^\top \in \mathbb{R}^{2n_L}$ . with  $\mathbf{e}_{\text{true}}, \mathbf{e}_p$  as indicator vectors for the target output.

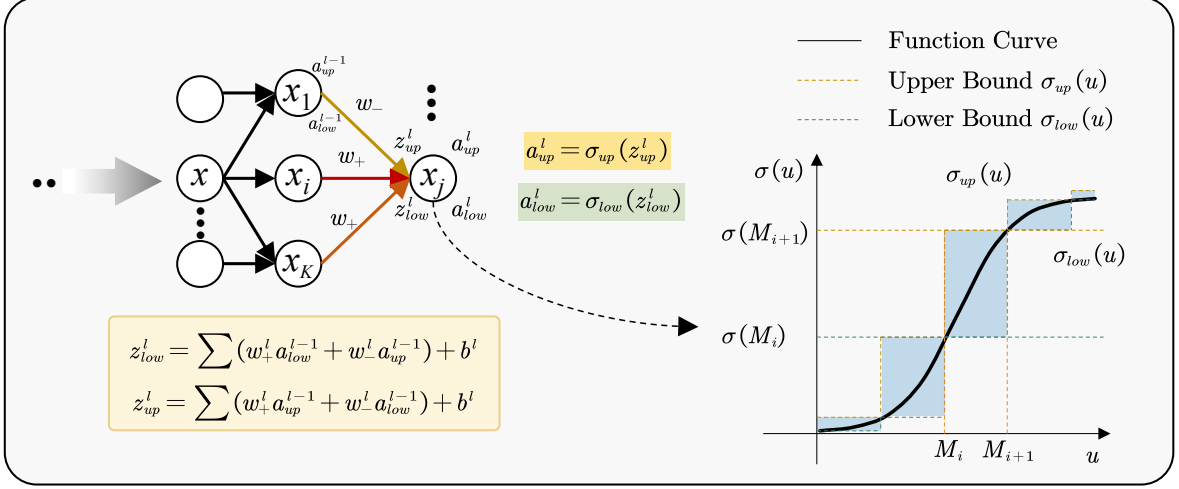


Figure 3: Illustration of the piecewise constant approximation for arbitrary non-linear activation functions. The non-linear function is bounded by upper and lower step functions, enabling verification with asymptotic completeness using Ising solver.

The problem is subject to constraints that propagate bounds through the network, modeled using binary variables  $\bar{\beta} = \{\bar{\beta}_{z_j^l}^{(i)}\}$  and  $\underline{\beta} = \{\underline{\beta}_{z_j^l}^{(i)}\}$  to select segments  $[M_{i-1}, M_i]$  for pre-activation upper and lower values  $\bar{z}_j^l, \underline{z}_j^l$ .

The constraints are expressed in matrix form for clarity and computational efficiency:

1. **Input Constraints:** The input  $\mathbf{x} = \mathbf{a}_x^0$  is constrained to an  $\ell_\infty$ -ball:

$$\begin{bmatrix} \mathbf{I}_{n_0} \\ -\mathbf{I}_{n_0} \end{bmatrix} \mathbf{x} \leq \begin{bmatrix} \mathbf{x}_0 + \varepsilon \mathbf{1} \\ -(\mathbf{x}_0 - \varepsilon \mathbf{1}) \end{bmatrix} = \mathbf{d}_{\text{input}}. \quad (15)$$

We proceed to present their integrated representation using the complete vector  $\mathbf{y}$ ,

$$\mathbf{C}_{\text{input}} \mathbf{y} \leq \mathbf{d}_{\text{input}},$$

where

$$\mathbf{C}_{\text{input}} = \begin{bmatrix} \mathbf{I}_{n_0} & \mathbf{0} & \cdots & \mathbf{0} \\ -\mathbf{I}_{n_0} & \mathbf{0} & \cdots & \mathbf{0} \end{bmatrix} \in \mathbb{R}^{2n_0 \times (n_0 + 4 \sum_{l=1}^L n_l)} \quad (16)$$

This constraint models adversarial perturbations, ensuring inputs remain close to  $\mathbf{x}_0$ , a cornerstone of robustness verification.

2. **Pre-activation Bounds:** For each layer  $l = 1, \dots, L$ , neuron  $j = 1, \dots, n_l$ , the pre-activation bounds are:

$$\bar{z}_j^l - \sum_{k:w_{jk}^l \geq 0} w_{jk}^l \bar{a}_k^{l-1} - \sum_{k:w_{jk}^l < 0} w_{jk}^l \underline{a}_k^{l-1} = b_j^l, \quad (17)$$

$$\underline{z}_j^l - \sum_{k:w_{jk}^l < 0} w_{jk}^l \underline{a}_k^{l-1} - \sum_{k:w_{jk}^l \geq 0} w_{jk}^l \bar{a}_k^{l-1} = b_j^l, \quad (18)$$

where  $w_{jk}^l$  are weights and  $b_j^l$  are biases. Define weight matrices:  $W_+^l \in \mathbb{R}^{n_l \times n_{l-1}}$  with  $(W_+^l)_{jk} = w_{jk}^l$  if  $w_{jk}^l \geq 0$ , else 0, and  $W_-^l \in \mathbb{R}^{n_l \times n_{l-1}}$  with  $(W_-^l)_{jk} = -w_{jk}^l$  if  $w_{jk}^l < 0$ , else 0. In matrix form:

$$\begin{bmatrix} \bar{\mathbf{z}}^l \\ \underline{\mathbf{z}}^l \end{bmatrix} - \begin{bmatrix} W_+^l & W_-^l \\ W_-^l & W_+^l \end{bmatrix} \begin{bmatrix} \bar{\mathbf{a}}^{l-1} \\ \underline{\mathbf{a}}^{l-1} \end{bmatrix} = \mathbf{b}_{\text{pre}}^l,$$

where  $\mathbf{b}_{\text{pre}}^l = [(\mathbf{b}^l)^\top, (\mathbf{b}^l)^\top]^\top \in \mathbb{R}^{2n_l}$ . We next formulate the overall constraints in matrix form with respect to the entire vector  $\mathbf{y}$ ,

$$\mathbf{A}_{\text{pre}}^l \mathbf{y} = \mathbf{b}_{\text{pre}}^l,$$

where the constraint matrix for layer  $l$  is

$$\mathbf{A}_{\text{pre}}^l = \begin{bmatrix} \mathbf{0} & \cdots & -W_{-}^l & -W_{+}^l & \mathbf{I}_{n_l} & \mathbf{0} & \mathbf{0} & \cdots \\ \mathbf{0} & \cdots & -W_{-}^l & -W_{+}^l & \mathbf{0} & \mathbf{I}_{n_l} & \mathbf{0} & \cdots \end{bmatrix} \in \mathbb{R}^{2n_l \times (n_0 + 4 \sum_{l=1}^L n_l)}.$$

This propagates bounds through linear transformations, using weight signs to compute worst-case pre-activations, critical for capturing the network's behavior under perturbations.

**3. Activation Bounds:** The activation bounds are:

$$\underline{a}_j^l = \sum_{i=1}^n \underline{\gamma}_i \underline{\beta}_{z_j^l}^{(i)}, \quad \bar{a}_j^l = \sum_{i=1}^n \bar{\gamma}_i \bar{\beta}_{z_j^l}^{(i)}, \quad \forall l, j, \quad (19)$$

where  $\underline{\gamma}_i, \bar{\gamma}_i$  are precomputed lower and upper values for segment  $i$ .

Define the binary variable matrices:

- $B_{\bar{\beta}}^l \in \mathbb{R}^{n_l \times n}$ :  $j$ -th row is  $\bar{\beta}_{z_j^l}^{\top} = [\bar{\beta}_{z_j^l}^{(1)}, \dots, \bar{\beta}_{z_j^l}^{(n)}]$ .
- $B_{\underline{\beta}}^l \in \mathbb{R}^{n_l \times n}$ :  $j$ -th row is  $\underline{\beta}_{z_j^l}^{\top} = [\underline{\beta}_{z_j^l}^{(1)}, \dots, \underline{\beta}_{z_j^l}^{(n)}]$ .

In matrix form:

$$\begin{bmatrix} \underline{\mathbf{a}}^l \\ \bar{\mathbf{a}}^l \end{bmatrix} = \mathbf{b}_{\text{act}}^l.$$

where  $\mathbf{b}_{\text{act}}^l = [ (B_{\underline{\beta}}^l \underline{\gamma})^{\top}, (B_{\bar{\beta}}^l \bar{\gamma})^{\top} ]^{\top}$ . We now synthesize the constraint into a comprehensive expression utilizing the full vector  $\mathbf{y}$ ,

$$\mathbf{A}_{\text{act}}^l \mathbf{y} = \mathbf{b}_{\text{act}}^l,$$

where

$$\mathbf{A}_{\text{act}}^l = \begin{bmatrix} \mathbf{0} & \cdots & \mathbf{I}_{n_l} & \mathbf{0} & \mathbf{0} & \mathbf{0} & \cdots \\ \mathbf{0} & \cdots & \mathbf{0} & \mathbf{I}_{n_l} & \mathbf{0} & \mathbf{0} & \cdots \end{bmatrix} \in \mathbb{R}^{2n_l \times (n_0 + 4 \sum_{l=1}^L n_l)}.$$

This models the piecewise constant behavior of upper and lower bounds of activation functions, fixing activations to specific values based on segment choices.

**4. Piecewise Linear Constraints:** Pre-activation values are constrained to segments  $[M_{i-1}, M_i]$ :

$$\bar{z}_j^l \geq \sum_{i=1}^n M_{i-1} \bar{\beta}_{z_j^l}^{(i)}, \quad \bar{z}_j^l \leq \sum_{i=1}^n M_i \bar{\beta}_{z_j^l}^{(i)}, \quad (20)$$

$$\underline{z}_j^l \geq \sum_{i=1}^n M_{i-1} \underline{\beta}_{z_j^l}^{(i)}, \quad \underline{z}_j^l \leq \sum_{i=1}^n M_i \underline{\beta}_{z_j^l}^{(i)}, \quad (21)$$

To derive a unified vector-matrix inequality, define the segment boundary vectors:

- $\mathbf{M}_{-} = [M_0, M_1, \dots, M_{n-1}]^{\top} \in \mathbb{R}^n$ ,
- $\mathbf{M}_{+} = [M_1, M_2, \dots, M_n]^{\top} \in \mathbb{R}^n$ .

The inequalities for  $\bar{\mathbf{z}}^l$  and  $\underline{\mathbf{z}}^l$  are:

$$\begin{bmatrix} -\mathbf{I}_{n_l} & \mathbf{0} \\ \mathbf{I}_{n_l} & \mathbf{0} \\ \mathbf{0} & -\mathbf{I}_{n_l} \\ \mathbf{0} & \mathbf{I}_{n_l} \end{bmatrix} \begin{bmatrix} \bar{\mathbf{z}}^l \\ \underline{\mathbf{z}}^l \end{bmatrix} \leq \begin{bmatrix} -B_{\bar{\beta}}^l \mathbf{M}_{-} \\ B_{\bar{\beta}}^l \mathbf{M}_{+} \\ -B_{\underline{\beta}}^l \mathbf{M}_{-} \\ B_{\underline{\beta}}^l \mathbf{M}_{+} \end{bmatrix} = \mathbf{d}_{\text{pwl}}^l \in \mathbb{R}^{4n_l}.$$

We now consolidate these into a unified matrix form expressed in terms of the full variable vector  $\mathbf{y}$ ,

$$\mathbf{C}_{\text{pwl}}^L \mathbf{y} \leq \mathbf{d}_{\text{pwl}}^l,$$

where

$$\mathbf{C}_{\text{pwl}}^L = \begin{bmatrix} \mathbf{0} & \cdots & \mathbf{0} & -\mathbf{I}_{n_l} & \mathbf{0} & \cdots \\ \mathbf{0} & \cdots & \mathbf{0} & \mathbf{I}_{n_l} & \mathbf{0} & \cdots \\ \mathbf{0} & \cdots & \mathbf{0} & \mathbf{0} & -\mathbf{I}_{n_l} & \cdots \\ \mathbf{0} & \cdots & \mathbf{0} & \mathbf{0} & \mathbf{I}_{n_l} & \cdots \end{bmatrix} \in \mathbb{R}^{4n_l \times (n_0 + 4 \sum_{l=1}^L n_l)}. \quad (22)$$

These constraints ensure pre-activations align with the selected segments, enforcing the piecewise structure.

## Theoretical Analysis

The performance of Model 2 hinges on the granularity of the piecewise constant approximation, controlled by the number of segments  $n$ . We analyze its convergence properties using the network’s Lipschitz constant, which quantifies the maximum rate of change of the output with respect to the input, providing a measure of sensitivity to perturbations.

**Theorem 1** (Convergence to Exact Bounds). *Let  $f(\mathbf{x})$  be the output of a DNN with an arbitrary activation function  $\sigma(z)$ , and let  $L$  be the global Lipschitz constant of the network, defined as  $L = \sup_{\mathbf{x}, \mathbf{x}' \in \mathcal{X}} \frac{\|f(\mathbf{x}) - f(\mathbf{x}')\|}{\|\mathbf{x} - \mathbf{x}'\|}$ , where  $\mathcal{X}$  is the input domain. For Model 2, as the number of segments  $n$  increases such that the maximum segment width  $\Delta = \max_i(M_i - M_{i-1}) \leq \frac{\epsilon}{L \cdot C}$ , where  $C$  is a constant depending on the network depth and activation smoothness, the computed bounds  $\underline{a}_0^L$  and  $\bar{a}_0^L$  converge to the true minimum and maximum output values over the  $\ell_\infty$ -ball  $\|\mathbf{x} - \mathbf{x}_0\|_\infty \leq \epsilon$ .*

## Approaches for Spin Complexity Reduction

### Interval Arithmetic for Pre-estimating Neuron Input Bounds

To enhance the computational efficiency of our approach for neural network robustness verification, we employ interval arithmetic to pre-estimate the input intervals of neurons. This preprocessing step allows us to exclude infeasible segments, thereby setting corresponding binary variables  $\bar{\beta}_{z_j^l}^{(i)}$  and  $\underline{\beta}_{z_j^l}^{(i)}$  to zero, reducing the combinatorial complexity of the master problem.

Interval arithmetic propagates bounds through the network by considering the range of possible values for each neuron’s pre-activation  $z_j^l$ . Given the input  $\mathbf{x}$  constrained within an  $\ell_\infty$ -ball of radius  $\epsilon$  around  $\mathbf{x}_0$ , the initial interval for  $\mathbf{x}$  is  $[\mathbf{x}_0 - \epsilon \mathbf{1}, \mathbf{x}_0 + \epsilon \mathbf{1}]$ . For layer  $l$ , the pre-activation  $z_j^l = \sum_k w_{jk}^l a_k^{l-1} + b_j^l$  is computed using interval operations, where  $a_k^{l-1} \in [\underline{a}_k^{l-1}, \bar{a}_k^{l-1}]$ . The interval  $[z_{j,\min}^l, z_{j,\max}^l]$  is obtained as:

$$z_{j,\min}^l = \sum_{k:w_{jk}^l \geq 0} w_{jk}^l \underline{a}_k^{l-1} + \sum_{k:w_{jk}^l < 0} w_{jk}^l \bar{a}_k^{l-1} + b_j^l, \quad (23)$$

$$z_{j,\max}^l = \sum_{k:w_{jk}^l \geq 0} w_{jk}^l \bar{a}_k^{l-1} + \sum_{k:w_{jk}^l < 0} w_{jk}^l \underline{a}_k^{l-1} + b_j^l. \quad (24)$$

This process is iterated across all layers, yielding intervals for  $\underline{z}_j^l$  and  $\bar{z}_j^l$  based on the worst-case combinations of previous layer bounds. The precomputed intervals  $[z_{j,\min}^l, z_{j,\max}^l]$  are compared against the segment boundaries  $[M_{i-1}, M_i]$  for  $i = 1, \dots, n$ . If  $[z_{j,\min}^l, z_{j,\max}^l]$  does not intersect  $[M_{i-1}, M_i]$ , the segment is deemed infeasible. Specifically, for  $\bar{z}_j^l$  and  $\underline{z}_j^l$ , if  $\underline{z}_{j,\max}^l < M_{i-1}$  or  $\bar{z}_{j,\min}^l > M_i$ , set  $\bar{\beta}_{z_j^l}^{(i)}$  and  $\underline{\beta}_{z_j^l}^{(i)}$  to 0. This pre-estimation significantly reduces the search space by pruning segments that cannot be reached under the given perturbation bounds. For deep networks with many neurons, where the number of binary variables is  $2 \sum_{l=1}^L n_l \cdot n$ , excluding infeasible segments can decrease the combinatorial complexity, accelerating the master problem’s solution. The approach is particularly effective when the network’s weight distributions or input perturbations limit the feasible pre-activation ranges, as it leverages interval arithmetic’s conservatism to guarantee correctness while optimizing efficiency.

### Pruning-Induced Robustness Transfer

**Motivation.** Verification pipelines, including MILP, SMT, branch-and-bound, or quantum-amenable QUBO encodings, are sensitive to model size. *Pruning* removes parameters and typically shrinks parameter dynamic ranges, enabling lower bit-width arithmetic. This section provides a rigorous account of how verification results obtained on a pruned network can be transferred to the original model with quantifiable guarantees, and how these guarantees translate into concrete bit-width requirements.

**Setup.** Let  $f, g : \mathbb{R}^{n_0} \rightarrow \mathbb{R}^K$  denote the original and pruned networks’ logits, respectively, and define the *pruning residual*

$$\mathbf{r}(\mathbf{z}) = f(\mathbf{z}) - g(\mathbf{z}) \in \mathbb{R}^K.$$

For a labeled sample  $(\mathbf{x}, y)$ , define the logit margin functional

$$m(\mathbf{a}) := \mathbf{a}_y - \max_{k \neq y} \mathbf{a}_k, \quad \Phi_f(\mathbf{x}; \epsilon) := \inf_{\|\delta\|_p \leq \epsilon} m(f(\mathbf{x} + \delta)), \quad \Phi_g(\mathbf{x}; \epsilon) := \inf_{\|\delta\|_p \leq \epsilon} m(g(\mathbf{x} + \delta)).$$

**Uniform pruning error in the perturbation ball.** Assume there exists a computable  $\tau \geq 0$  such that

$$\|\mathbf{r}(\mathbf{x} + \boldsymbol{\delta})\|_\infty \leq \tau, \quad \forall \|\boldsymbol{\delta}\|_p \leq \varepsilon. \quad (25)$$

We will discuss the construction of such a  $\tau$  later in this section.

**A stability inequality.** For any  $\mathbf{a}, \mathbf{b} \in \mathbb{R}^K$  and label  $y$ ,

$$m(\mathbf{a} + \mathbf{b}) \geq m(\mathbf{a}) - 2\|\mathbf{b}\|_\infty, \quad m(\mathbf{a} + \mathbf{b}) \leq m(\mathbf{a}) + 2\|\mathbf{b}\|_\infty. \quad (26)$$

*Proof.* We use  $\max_{k \neq y} (a_k + b_k) \leq \max_{k \neq y} a_k + \max_j b_j$  and  $a_y + b_y \geq a_y - \|\mathbf{b}\|_\infty$  to get the lower bound; the upper bound is analogous.  $\square$

**Theorem 2** (Pruning-induced robustness transfer). Fix  $(\mathbf{x}, y)$ , a norm  $\|\cdot\|_p$ , and radius  $\varepsilon$ . Under (25),

$$\Phi_g(\mathbf{x}; \varepsilon) - 2\tau \leq \Phi_f(\mathbf{x}; \varepsilon) \leq \Phi_g(\mathbf{x}; \varepsilon) + 2\tau. \quad (27)$$

Consequently, for any computable lower and upper bounds  $L_g(\mathbf{x}; \varepsilon) \leq \Phi_g(\mathbf{x}; \varepsilon)$ ,  $U_g(\mathbf{x}; \varepsilon) \geq \Phi_g(\mathbf{x}; \varepsilon)$ ,

$$\Phi_f(\mathbf{x}; \varepsilon) \geq L_g(\mathbf{x}; \varepsilon) - 2\tau, \quad \Phi_f(\mathbf{x}; \varepsilon) \leq U_g(\mathbf{x}; \varepsilon) + 2\tau.$$

In particular, if  $L_g(\mathbf{x}; \varepsilon) > 2\tau$ , then  $\Phi_f(\mathbf{x}; \varepsilon) > 0$  and  $(\mathbf{x}, y)$  is certifiably robust for  $f$ ; if  $U_g(\mathbf{x}; \varepsilon) \leq -2\tau$ , then  $\Phi_f(\mathbf{x}; \varepsilon) \leq 0$  and  $(\mathbf{x}, y)$  is provably non-robust for  $f$ .

The proof is included in Appendix B.

**Consequences for dataset-level certification.** For a dataset  $S$ , any verifier providing bounds  $(L_g, U_g)$  for  $g$  induces

$$\underline{\text{CA}}_f(\varepsilon) = \frac{1}{|S|} \sum_{(\mathbf{x}, y) \in S} \mathbf{1}\{L_g(\mathbf{x}; \varepsilon) > 2\tau\} \leq \text{CA}_f(\varepsilon) \leq 1 - \frac{1}{|S|} \sum_{(\mathbf{x}, y) \in S} \mathbf{1}\{U_g(\mathbf{x}; \varepsilon) \leq -2\tau\} = \overline{\text{CA}}_f(\varepsilon).$$

Thus, verification on the *easier* pruned model  $g$  controls certification for  $f$  up to a safety buffer  $2\tau$ .

**Network and pruning model.** Consider a feedforward network with 1-Lipschitz activation  $\sigma$  (e.g. ReLU/Leaky-ReLU; or scaled tanh with Lipschitz constant  $\leq 1$ ):

$$\mathbf{z}_l = \mathbf{W}_l \mathbf{h}_{l-1} + \mathbf{b}_l, \quad \mathbf{h}_l = \sigma(\mathbf{z}_l), \quad l = 1, \dots, L,$$

and logits  $f(\mathbf{u}) = \mathbf{z}_L(\mathbf{u})$  (or  $\mathbf{h}_L$  depending on convention; the derivation is identical). Structured/unstructured pruning replaces  $\mathbf{W}_l$  by  $\mathbf{W}'_l = \mathbf{W}_l \odot \mathbf{M}_l$  (Hadamard mask), and define

$$\Delta \mathbf{W}_l := \mathbf{W}_l - \mathbf{W}'_l = \mathbf{W}_l \odot (\mathbf{1} - \mathbf{M}_l).$$

Let  $g$  denote the pruned network using  $\mathbf{W}'_l$ . We can construct the following bound on  $\tau$ ,

$$\tau \leq \sum_{l=1}^L \left( \prod_{j=l+1}^L \|\mathbf{W}'_j\|_{\infty \rightarrow \infty} \right) \|\Delta \mathbf{W}_l\|_{\infty \rightarrow \infty} H_{l-1}. \quad (28)$$

The details are included in Appendix C.

The expression (28) is small when

- The removed row-wise  $\ell_1$ -mass is small. If each row  $i$  has a small removed  $\ell_1$ -mass, i.e.  $\sum_{j:(M_l)_{ij}=0} |(W_l)_{ij}|$  is small uniformly over  $i$ , then  $\|\Delta \mathbf{W}_l\|_{\infty \rightarrow \infty}$  is small;
- the pruned network is well-conditioned, so  $\|\mathbf{W}'_j\|_{\infty \rightarrow \infty}$  does not blow up;
- pruning *later layers* tends to reduce  $\tau$  more because the multiplicative prefix  $\prod_{j=l+1}^L \|\mathbf{W}'_j\|_{\infty \rightarrow \infty}$  is shorter;
- the verifier produces tight intermediate bounds  $H_{l-1}$  on the perturbation ball.

---

**Algorithm 1** Verification-Aware Pruning for Robustness Transfer

---

**Require:** Original network  $f$ ; pruning masks  $\{\mathbf{M}_l\}_{l=1}^L$ ; dataset  $S$ ; norm  $\|\cdot\|_p$ ; radius  $\varepsilon$ ; verifier  $\mathcal{V}$

**Ensure:** Lower and upper certified accuracy bounds  $\underline{\text{CA}}_f(\varepsilon), \overline{\text{CA}}_f(\varepsilon)$

- 1: Construct pruned weights  $\mathbf{W}'_l = \mathbf{W}_l \odot \mathbf{M}_l$ , and residuals  $\Delta\mathbf{W}_l = \mathbf{W}_l - \mathbf{W}'_l$
  - 2: **for** each sample  $(\mathbf{x}, y) \in S$  **do**
  - 3:   Compute activation bounds  $H_{l-1}(\mathbf{x})$  on  $\{\mathbf{x} + \boldsymbol{\delta} : \|\boldsymbol{\delta}\|_p \leq \varepsilon\}$
  - 4:   Compute an estimation of
  - 5:    $\tau(\mathbf{x}) \leftarrow \sum_{l=1}^L \left( \prod_{j=l+1}^L \|\mathbf{W}'_j\|_{\infty \rightarrow \infty} \right) \|\Delta\mathbf{W}_l\|_{\infty \rightarrow \infty} H_{l-1}(\mathbf{x})$
  - 6:   Run verifier  $\mathcal{V}$  on  $g$  to obtain  $L_g(\mathbf{x}; \varepsilon), U_g(\mathbf{x}; \varepsilon)$
  - 7: **end for**
  - 8:  $\underline{\text{CA}}_f(\varepsilon) \leftarrow \frac{1}{|S|} \sum_{(\mathbf{x}, y) \in S} \mathbf{1}\{L_g(\mathbf{x}; \varepsilon) > 2\tau(\mathbf{x})\}$
  - 9:  $\overline{\text{CA}}_f(\varepsilon) \leftarrow 1 - \frac{1}{|S|} \sum_{(\mathbf{x}, y) \in S} \mathbf{1}\{U_g(\mathbf{x}; \varepsilon) \leq -2\tau(\mathbf{x})\}$
- 

## Scalable Robustness Verification via Layerwise Partitioning and CIM-Assisted Solving

A principal barrier to scaling quantum-assisted robustness verification is the *bit budget*: encoding all network parameters, intermediate activations, and verification certificates into a single QUBO/Ising instance easily exhausts the available spins on current coherent Ising machines (CIMs). We propose a *layerwise partitioning* scheme that separates the network into a prefix handled classically by sound over-approximation (interval or linear-relaxation propagation), and a suffix solved on quantum hardware using the QUBO model developed earlier. This reduces the number of binary variables required on the CIM while preserving correctness guarantees.

**Setup.** Let  $f = f_L \circ f_{L-1} \circ \dots \circ f_1$  be an  $L$ -layer feedforward network. Fix a perturbation model  $\mathcal{B}(x_0)$  around a nominal input  $x_0$  (e.g., an  $\ell_p$ -ball). Choose a *cut index*  $\tau \in \{1, \dots, L-1\}$  and denote the *prefix*  $\text{P} := f_\tau \circ \dots \circ f_1$  and the *suffix*  $\text{S} := f_L \circ \dots \circ f_{\tau+1}$ . For an input set  $X \subseteq \mathbb{R}^d$ , write the prefix reachable set as

$$\mathcal{R}_\tau(X) := \{z \in \mathbb{R}^{m_\tau} : \exists x \in X, z = \text{P}(x)\}.$$

Since computing  $\mathcal{R}_\tau(X)$  exactly is hard, we construct a sound outer approximation  $\widehat{\mathcal{R}}_\tau(X) \supseteq \mathcal{R}_\tau(X)$  by *classical bound propagation*. In its simplest form (interval bound propagation, IBP), for each neuron  $j$  at layer  $\tau$  we compute intervals  $[\underline{z}_j, \bar{z}_j]$  and set

$$\widehat{\mathcal{R}}_\tau(X) := \prod_{j=1}^{m_\tau} [\underline{z}_j, \bar{z}_j].$$

Tighter relaxations (e.g., linear zonotopes, CROWN-type linear bounds) can be substituted without changing the flow below.

**Suffix-side QUBO on the CIM.** With the prefix abstracted as the input set  $\widehat{\mathcal{R}}_\tau(X)$ , we verify the property of interest only on the suffix. For the untargeted robustness of a classifier with correct label  $y$ , a standard margin form is

$$\gamma \equiv \min_{z \in \widehat{\mathcal{R}}_\tau(X)} \max_{y' \neq y} \left( S_{y'}(z) - S_y(z) \right). \quad (29)$$

Using the QUBO construction for (29) in Section , the resulting QUBO is solved on CIM. A nonnegative optimum of (29) certifies robustness of the full network.

## Experimental Evaluation

This section provides a comprehensive experimental evaluation of our robustness verification framework. The study is structured to assess both correctness and practical viability under two complementary regimes: (i) global QUBO-based verification, which directly tests the performance of our encoding, and (ii) scalable verification via a quantum-classical hybrid decomposition strategy, which targets larger problem instances. Across all experiments, we consider two verification models: Model 1, which yields exact certification for networks with piecewise-linear (PWL) activations, and Model 2, which extends verification to general nonlinear activations via controlled approximations.

**Datasets and Networks.** We use two datasets to probe verification behavior at different scales. To validate the QUBO formulation, we train a shallow feedforward network on the Iris dataset [25]. To evaluate scalability, we train a larger network on the make\_moons dataset [26], whose nonlinear decision boundary induces more challenging verification instances. Both datasets are generated and processed using scikit-learn [26]. We emphasize that the purpose of these experiments is to establish the feasibility and effectiveness of quantum optimization as a verification primitive, rather than to claim immediate computational superiority over state-of-the-art classical solvers.

For global QUBO verification, we evaluate on 100 Iris test samples, balanced across the two classes. For the Benders-based scalability experiments, we evaluate on 100 make\_moons test samples, likewise in a balanced binary classification setting. We instantiate Model 1 with ReLU and hardtanh activations, enabling exact verification for PWL networks, and instantiate Model 2 with the sigmoid activation to evaluate verification of nonlinear networks via approximation.

All networks are trained with the Adam optimizer [27] using a learning rate of 0.01. Given the small sample sizes (on the order of 100 samples per dataset), we train in full-batch mode for 100 epochs, ensuring convergence. Each trained model achieves 100% accuracy on the corresponding clean test set, isolating robustness verification effects from classification error.

Approach	Method	Activation	Property	
			Sound	Complete
Optimization	BaB [15]	ReLU	✓	✓
	ConvDual [11]	ReLU	✓	×
	Duality [28]	monotonic	✓	×
	NSVerify [29]	ReLU	✓	✓
	Reluplex [13]	ReLU	✓	✓
	Sherlock [30]	ReLU	✓	×
Reachability	AI2 [31]	ReLU	✓	×
	DLV [32]	any	✓	×
	ExactReach [33]	ReLU	✓	✓
	FastLin [34]	ReLU	✓	×
	FastLip [34]	ReLU	✓	×
	MaxSens [35]	monotonic	✓	×
	Neurify [16]	ReLU	✓	×
ReluVal [36]	ReLU	✓	×	

Table 2: Comparison of Verification Methods

**Verification Methods.** We compare our framework against several representative baselines. MIP-Gurobi is the primary reference method: it encodes robustness verification as a monolithic mixed-integer program (MIP) and solves it using the Gurobi optimizer [37]. To evaluate our QUBO formulation independently of the solver, we solve the resulting QUBOs with both Gurobi (QUBO-Gurobi) and a Coherent Ising Machine (QUBO-CIM), enabling a controlled comparison between a classical optimizer and a quantum-inspired Ising solver on an identical problem encoding. Finally, we evaluate our Benders-decomposition-based quantum-classical hybrid algorithm, which is designed to improve scalability on larger networks. Across all methods, we employ Interval Bound Propagation (IBP) as a fast pre-screening step: instances certified by IBP are terminated early, while the remaining unresolved instances are passed to the corresponding verifier.

All experiments consider  $\ell_\infty$ -bounded adversarial perturbations. We vary the perturbation radius  $\epsilon$  to probe performance under increasing verification difficulty. For the global QUBO experiments, we sweep  $\epsilon \in [0.1, 0.6]$ . For the Benders-decomposition experiments, we use a finer grid with  $\epsilon \in [0.05, 0.5]$ , enabling a more granular characterization of scaling behavior as the perturbation budget increases.

To situate our approach relative to established classical verification techniques, we additionally compare against several optimization- and reachability-based baselines summarized in Table 2. These methods span different theoretical properties (e.g., soundness/completeness) and supported activation families. Since many prior verifiers are specialized to ReLU networks, for hardtanh and sigmoid we restrict attention to methods that remain applicable beyond ReLU, namely Duality [28] and MaxSens [35], which can accommodate monotone or more general activation functions.

**Evaluation Metrics.** We evaluate the proposed framework using two metrics: (i) the number of vulnerable samples identified by the algorithm, and (ii) the certified accuracy. These metrics reflect both the practical effectiveness of vulnerable sample discovery and the theoretical reliability of the verification process.

When the CIM is used as a direct solver, we adopt the number of discovered counterexamples as the primary metric, since the hardware does not provide certificates of global optimality. However, robustness falsification does not require optimal solutions, the existence of any feasible solution that violates the specification, including suboptimal ones, suffices to establish a counterexample. Therefore, the ability of the CIM to efficiently identify such solutions makes the number of vulnerable samples a natural and practically meaningful performance indicator. In contrast, when Benders decomposition is incorporated, the framework is able to provide rigorous upper and lower bounds on the objective value. These bounds enable certification of either infeasibility or optimality, thereby supporting conclusive robustness verification. In this setting, verification accuracy becomes a well-defined and theoretically grounded metric, as the availability of bounds allows us to determine whether the absence of counterexamples is due to true robustness or merely incomplete search.

**Experimental Environment and Hardware Configuration.** We solve QUBO instances on a Coherent Ising Machine (CIM) [38], while all classical components are executed on an Apple M4 CPU (10-core). For QUBO construction, we first apply Interval Bound Propagation (IBP) to estimate per-variable ranges. This preprocessing yields instance-dependent encodings: even at a fixed perturbation budget  $\epsilon$ , different test samples can induce different bounds and, consequently, require different numbers of Ising spins. For Model 2, we approximate the sigmoid activation with a 5-segment piecewise-constant enclosure. Because robustness verification assumes the ground-truth label is known, Model 2 reduces to a one-sided check (upper or lower bound), which further decreases the number of spin variables.

Perturbation Budget $\epsilon$		0.1	0.2	0.3	0.4	0.5	0.6
Vulnerable Samples ↑	AI2 [31]	0	0	0	3	6	12
	DLV [32]	0	0	0	2	6	12
	ExactReach [33]	0	0	0	2	6	12
	MaxSens [35]	0	0	0	3	6	12
	Neurify [16]	0	0	0	2	6	12
	BaB [15]	0	0	0	2	6	12
	ConvDual [11]	0	0	0	2	6	12
	Duality [28]	0	0	0	2	6	12
	ILP [39]	0	0	0	2	6	11
	NSVerify [29]	0	0	0	2	6	12
	Reluplex [13]	0	0	0	2	6	12
	Sherlock [30]	0	0	0	2	6	12
	MIP-Gurobi	0	0	0	2	6	12
	QUBO-Gurobi	0	0	0	2	6	12
	QUBO-CIM	0	0	0	2	6	12
Time (ms)↓	MIP-Gurobi	0.526	0.305	0.33	0.361	0.369	0.443
	QUBO-Gurobi	1137	Timeout at 5000 ms				
	QUBO-CIM (evolutionary time)	2.496	2.602	2.755	11.966	2.799	8.489
Ising Spins	Average	198.03	240.89	255.72	300.25	320.63	338.28
	Max	304	379	384	494	497	531
	Min	102	116	120	139	143	196

Table 3: Verification Results for ReLU Network

**ReLU networks.** Table 3 reports certification outcomes for ReLU networks. For every perturbation budget  $\epsilon$ , the number of vulnerable samples identified by QUBO-Gurobi and QUBO-CIM exactly matches the MIP-Gurobi benchmark. This yields two key takeaways. First, the agreement between QUBO-Gurobi and MIP-Gurobi provides evidence that our QUBO encoding is semantically faithful to the underlying verification problem, it could preserve the existence of adversarial solutions. Second, the computational profiles differ sharply. Despite identifying the same number of vulnerable samples, QUBO-Gurobi is substantially slower than MIP-Gurobi, often by orders of magnitude. For example, at  $\epsilon = 0.5$ , QUBO-Gurobi consistently exceeds the 5-second timeout,

whereas MIP-Gurobi completes in 0.369 ms. Indeed, QUBO-Gurobi reaches the timeout threshold for all  $\epsilon \geq 0.2$ , indicating that the QUBO-induced structure is difficult for a general-purpose classical solver when applied directly to the unconstrained binary formulation.

By contrast, the CIM identifies the same number of vulnerable samples as MIP-Gurobi while requiring less time than QUBO-Gurobi. Its ability to solve QUBO instances that are effectively intractable for the classical solver under the imposed time budget, provides empirical support for the premise that Ising-type solver can better exploit the combinatorial structure arising in QUBO-based neural network verification. Exact verifiers, including BaB [15], NSVerify [29], and Reluplex [13], report the same number of vulnerable samples as MIP-Gurobi, consistent with their theoretical completeness guarantees. By contrast, AI2 [31] and MaxSens [35] report a larger number of vulnerable samples at  $\epsilon = 0.4$ . This discrepancy arises because these methods are incomplete and may produce unsound adversarial detections due to relaxation or approximation errors, leading to false positives.

## Verification via Global QUBO Formulation

We first evaluate the global QUBO formulation on a shallow network trained on the Iris dataset. Model 1 targets sound and complete robustness verification for networks with piecewise-linear (PWL) activations. The results below validate both the correctness of the formulation and its empirical behavior.

We also characterize the Ising spin complexity induced by the global QUBO encoding for ReLU networks. As  $\epsilon$  increases from 0.1 to 0.6, the mean number of spins rises from 198 to 338, while the maximum increases from 304 to 531 and the minimum from 102 to 196. This monotone growth matches the expected scaling behavior: larger perturbation radius widen feasible variable ranges, which in turn requires finer binary representations and increases the discrete search space. Finally, the gap between the minimum, mean, and maximum spin counts underscores the instance-dependent nature of verification difficulty, driven primarily by sample-specific IBP range estimates that directly determine encoding tightness and binary-variable requirements.

**Hardtanh networks.** To assess generality beyond ReLU, we further evaluate Model 1 on networks with hardtanh activations. Although hardtanh is also piecewise linear, it differs structurally from ReLU by introducing two saturation breakpoints at  $-1$  and  $1$ , which induces a distinct feasible-region geometry in the verification program.

As shown in Table 4, the hardtanh results closely track the trends observed for ReLU. For every perturbation budget  $\epsilon$ , MIP-Gurobi provides the reference number of vulnerable samples, against which other methods are compared. QUBO-Gurobi identifies fewer vulnerable samples than MIP-Gurobi at larger perturbation budgets (e.g.,  $\epsilon \geq 0.5$ ). This gap is not due to modeling discrepancies, but rather to the imposed 5-second time limit. This behavior indicates that the unconstrained binary encoding remains challenging for a general-purpose classical solver under given computational budgets. In contrast, QUBO-CIM recovers nearly the same number of vulnerable samples as MIP-Gurobi across all  $\epsilon$ , despite the same time constraints, demonstrating its effectiveness in discovering valid counterexamples within limited runtime.

Perturbation Budget $\epsilon$		0.1	0.2	0.3	0.4	0.5	0.6	0.7	0.8	0.9	1.0
Vulnerable Samples ↑	Duality [28]	0	0	0	3	12	24	43	52	59	70
	MaxSens [35]	0	0	0	3	12	24	43	52	59	70
	MIP-Gurobi	0	0	0	2	11	21	41	52	59	66
	QUBO-Gurobi	0	0	0	2	10	19	36	46	50	61
	QUBO-CIM	0	0	0	2	11	21	40	50	57	60
Time (ms)↓	MIP-Gurobi	0.645	0.414	0.473	0.493	0.575	0.728	0.809	0.716	0.545	0.652
	QUBO-Gurobi	1096				Timeout at 5000 ms					
	QUBO-CIM (evolutionary time)	2.195	1.792	2.386	2.478	6.522	3.854	9.556	10.390	9.747	10.113
Ising Spins	Average	192.39	226.69	235.50	284.13	293.93	303.62	343.77	372.32	391.64	402.71
	Max	252	296	297	335	337	340	446	453	487	492
	Min	158	179	204	237	238	238	270	335	336	338

Table 4: Verification Results for Hardtanh Network

Among the non-exact baselines applicable to hardtanh, Duality [28] and MaxSens [35] report a strictly larger number of vulnerable samples than MIP-Gurobi for  $\epsilon \geq 0.4$ . Again this discrepancy arises because these methods are incomplete and thus may introduce spurious adversarial solutions. Consequently, the number of counterexamples they report constitutes an upper bound on the true number of vulnerable samples, rather than an exact count.

Overall, these findings demonstrate that our approach is not tailored to the specific algebraic structure of ReLU. By closely matching the reference vulnerable-sample counts produced by the complete MIP formulation,

Model 1 preserves the exact adversarial solution structure even under a qualitatively different PWL nonlinearity. Moreover, despite  $\text{hardtanh}$ 's more intricate breakpoint structure, the resulting Ising spin complexity remains comparable to that of ReLU, further supporting Model 1's suitability for diverse PWL networks under realistic hardware constraints.

Model 2 targets robustness verification for networks with arbitrary nonlinear activation functions via piecewise-constant enclosures, yielding a sound over-approximation with asymptotic completeness as the segmentation is refined. We evaluate Model 2 on a network with sigmoid activations.

**Sigmoid Network.** Table 5 summarizes the verification results. A central difficulty in approximation-based verification is the trade-off between scalability and tightness: overly conservative bounds can dramatically reduce certified accuracy, undermining practical value. Despite operating on a piecewise-constant over-approximation, Model 2 identifies the same number of vulnerable samples as the exact MIP-Gurobi baseline across almost all perturbation budgets. Notably, even with a coarse 5-segment approximation, the vulnerable-sample counts match those of MIP-Gurobi and other baselines (with only a marginal one-sample deviation at  $\epsilon = 0.8$  for QUBO-CIM), demonstrating that the approximation introduces negligible distortion in counterexample detection. The two incomplete baselines, Duality and MaxSens, report identical vulnerable-sample counts to MIP-Gurobi in this experiment. However, as incomplete methods based on relaxation, their reported counterexample counts should be interpreted as upper bounds on the true number of vulnerable samples, since false positives cannot be ruled out in general.

Runtime trends provide additional insights. For sigmoid networks, MIP-Gurobi exhibits a modest increase in runtime compared to the piecewise-linear cases, with solve times consistently around 0.9–1.2 ms across perturbation budgets. While still efficient, this increase reflects the added modeling complexity induced by nonlinear activations.

Perturbation Budget $\epsilon$		0.1	0.2	0.3	0.4	0.5	0.6	0.7	0.8	0.9	1.0	
Vulnerable Samples ↑	Duality [28]	0	0	0	2	5	10	26	53	67	79	
	MaxSens [35]	0	0	0	2	5	10	26	53	67	79	
	MIP-Gurobi	0	0	0	2	5	10	26	53	67	79	
	QUBO-Gurobi	0	0	0	2	5	10	26	53	67	79	
	QUBO-CIM	0	0	0	2	5	10	26	52	67	79	
Time (ms)↓	MIP-Gurobi	0.983	0.885	1.000	0.927	1.179	1.034	1.104	1.169	1.066	1.227	
	QUBO-Gurobi	3367				Timeout at 5000 ms						
	QUBO-CIM (evolutionary time)	2.240	2.584	2.535	2.545	4.573	3.295	4.379	3.683	4.370	3.078	
Ising Spins	Average	64.37	74.55	79.92	85.38	90.67	91.88	96.88	97.64	100.49	103.49	
	Max	69	79	84	88	94	94	99	100	104	107	
	Min	60	71	78	83	89	89	95	95	99	101	

Table 5: Verification Results for Sigmoid Network

Model 2 exhibits a clear advantage in spin complexity. For the global QUBO formulation of sigmoid networks, the mean number of Ising spins increases only modestly, from 64 at  $\epsilon = 0.1$  to 92 at  $\epsilon = 0.6$ , with the maximum rising from 69 to 94 and the minimum from 60 to 89. These requirements are markedly lower than those observed for Model 1 (ReLU and  $\text{hardtanh}$ ). The reduction is driven by the design choice that the piecewise-constant enclosure removes the linearization procedure inherent to PWL encodings, simplifying the optimization landscape. In addition, exploiting known sample labels reduces verification to a one-sided check (either an upper or a lower bound), thereby minimizing the encoding burden. Notably, spin complexity varies little across samples under Model 2, indicating stable resource usage. Together, these results highlight Model 2 as particularly well-suited for certifying nonlinear networks on quantum hardware with limited spin budgets.

## Verification via Quantum-Classical Hybrid Algorithms

The global QUBO experiments establish both the correctness of our encoding and the practical efficacy of the CIM solver. To scale verification beyond the regime where global formulations remain tractable, we verify the strategy based on Benders decomposition. This scheme decouples discrete decisions from continuous optimization by alternately solving a master problem and its associated subproblems. The experiments below evaluate whether this decomposition preserves verification fidelity, namely, whether the hybrid procedure returns the same certification decisions as an exact MIP baseline.

Certified Accuracy (%) $\uparrow$		Perturbation Budget $\epsilon$									
		0.05	0.1	0.15	0.2	0.25	0.3	0.35	0.4	0.45	0.5
ReLU	AI2 [31]	99	98	97	95	93	89	70	46	30	25
	FastLin [34]	99	98	97	95	93	89	70	46	30	25
	FastLip [34]	99	98	97	95	93	89	70	46	30	25
	MaxSens [35]	98	89	64	37	15	9	6	2	0	0
	Neurify [16]	100	99	97	97	95	92	85	69	49	36
	ReluVal [36]	99	98	97	94	89	81	64	43	31	25
	BaB [15]	100	99	97	97	95	92	85	68	49	36
	NSVerify [29]	100	99	97	97	95	92	85	69	49	36
	Reluplex [13]	100	99	97	97	95	92	85	69	49	36
	Sherlock [30]	99	98	97	95	93	90	74	59	37	29
	MIP	100	99	97	97	95	92	85	69	49	36
	Benders	100	99	97	97	95	92	85	69	49	36
Hardtanh	Duality [28]	99	93	79	47	42	38	29	19	8	0
	DLV [32]	99	93	79	47	42	38	29	19	8	0
	MaxSens [35]	99	91	73	41	38	33	26	15	6	0
	MIP	100	100	99	97	95	92	89	82	72	49
	Benders	100	100	99	97	95	92	89	82	72	49
Sigmoid	Duality [28]	100	95	84	74	63	49	44	36	26	19
	DLV [32]	100	95	84	74	63	49	44	36	26	19
	MaxSens [35]	100	90	78	67	56	44	39	32	22	12
	MIP	100	96	85	76	66	52	46	38	31	21
	Benders	100	96	85	76	66	52	46	38	30	21

Table 6: Verification Results of Benders Algorithm

Table 6 reports certification outcomes for ReLU, hardtanh, and sigmoid networks under the Benders-based hybrid framework. For the piecewise-linear settings (ReLU and hardtanh), Benders attains certified accuracy identical to the MIP baseline for every perturbation budget  $\epsilon$ , indicating that the decomposition leaves the verification outcome unchanged. For the nonlinear sigmoid setting (Model 2), Benders closely tracks the MIP results across all  $\epsilon$ , with the maximum discrepancy limited to 1% (at  $\epsilon = 0.45$ ). Taken together, the near-perfect agreement with the exact MIP baseline across diverse activation families provides empirical support that the proposed quantum-classical Benders decomposition scales verification while preserving correctness in practice.

## Discussions

The central objective of this work is to establish the feasibility and correctness of quantum-optimization-based verification, rather than to claim immediate wall-clock dominance over highly optimized classical solvers. Our framework is modular and solver-agnostic, providing a clean interface for substituting increasingly powerful sub-problem engines, especially quantum solvers as they become available. As quantum hardware advances and spin budgets expand, we anticipate that the proposed pipeline will yield meaningful gains on larger networks, offering a principled route toward scalable robustness certification and helping lay the foundations for quantum-enabled verification in safety-critical AI systems.

We propose a quantum-optimization framework for certifying adversarial robustness of DNNs that supports both exact verification for piecewise-linear networks and scalable, asymptotically complete over-approximations for general nonlinear activations. By integrating Quantum Benders Decomposition, interval arithmetic, and resource-aware strategies such as certificate transfer from pruned models and layerwise quantum-classical partitioning, our approach mitigates the combinatorial and encoding overhead that limits existing methods. Experimental results validate the practicality of the framework and show competitive certification performance against classical baselines. Together, these contributions position quantum optimization as a promising pathway toward rigorous and scalable robustness guarantees for neural network systems.

## Methods

### QUBO Formulation and Quantum-Classical Hybrid Algorithm

We consider a compact representation of all decision variables arising in the formulation of the neural network verification problem. Let  $\mathbf{y} = [\mathbf{x}, \underline{\mathbf{a}}^1, \bar{\mathbf{a}}^1, \underline{\mathbf{z}}^1, \bar{\mathbf{z}}^1, \dots, \underline{\mathbf{a}}^L, \bar{\mathbf{a}}^L, \underline{\mathbf{z}}^L, \bar{\mathbf{z}}^L]^\top \in \mathbb{R}^{n_0+4\sum_{l=1}^L n_l}$ ,  $\mathbf{y}^L = [\underline{\mathbf{a}}^L, \bar{\mathbf{a}}^L]^\top \in \mathbb{R}^{2n_L}$  and  $\mathbf{c} = [\mathbf{e}_{\text{true}}, -\mathbf{e}_p]^\top \in \mathbb{R}^{2n_L}$ . Here,  $\mathbf{x} \in \mathbb{R}^{n_0}$  denotes the perturbed input variables, while  $\underline{\mathbf{a}}^l, \bar{\mathbf{a}}^l \in \mathbb{R}^{n_l}$  represent the lower and upper bounds of the pre-activation variables at layer  $l$ , respectively. Similarly,  $\underline{\mathbf{z}}^l, \bar{\mathbf{z}}^l \in \mathbb{R}^{n_l}$  denote the corresponding post-activation bounds induced by the activation relaxation. The vector  $\mathbf{y}^L$  collects the activation bounds at the final layer, which directly determine the classification margin. Given binary variables  $\bar{\boldsymbol{\beta}}$  and  $\underline{\boldsymbol{\beta}}$ , encoding the interval selection decisions associated with the activation patterns, the resulting subproblem can be written as follows,

$$\min_{\mathbf{y}} \quad \mathbf{c}^\top \mathbf{y}^L \quad (30)$$

$$\text{s.t.} \quad \mathbf{A}\mathbf{y} = \mathbf{b}(\bar{\boldsymbol{\beta}}, \underline{\boldsymbol{\beta}}), \quad (31)$$

$$\mathbf{C}\mathbf{y} \leq \mathbf{d}(\bar{\boldsymbol{\beta}}, \underline{\boldsymbol{\beta}}). \quad (32)$$

The equality constraints in (31) encode the affine transformations between consecutive layers, as well as the coupling between pre- and post-activation variables. The inequality constraints in (32) capture the activation functions together with the input perturbation set. The objective (30) minimizes the margin between the true class and a target class  $p$ , thereby certifying the existence of an adversarial example whenever the optimal value is negative.

For notational compactness, define the stacked vector  $\boldsymbol{\beta} = [\bar{\boldsymbol{\beta}}, \underline{\boldsymbol{\beta}}]^\top$ , and functions

$$\mathbf{b}(\bar{\boldsymbol{\beta}}, \underline{\boldsymbol{\beta}}) = \mathbf{b}_0 + \mathbf{B}\boldsymbol{\beta}, \quad (33)$$

$$\mathbf{d}(\bar{\boldsymbol{\beta}}, \underline{\boldsymbol{\beta}}) = \mathbf{d}_0 + \mathbf{D}\boldsymbol{\beta}, \quad (34)$$

with constant vectors  $\mathbf{b}_0, \mathbf{d}_0$  and coefficient matrices  $\mathbf{B}, \mathbf{D}$ . Let  $\mathbf{y}^L = \mathbf{S}\mathbf{y}$  and define  $\tilde{\mathbf{c}} \triangleq \mathbf{S}^\top \mathbf{c}$ . The formulation can then be written as

$$\min_{\mathbf{y}} \quad \tilde{\mathbf{c}}^\top \mathbf{y} \quad (35)$$

$$\text{s.t.} \quad \mathbf{A}\mathbf{y} = \mathbf{b}_0 + \mathbf{B}\boldsymbol{\beta}, \quad (36)$$

$$\mathbf{C}\mathbf{y} \leq \mathbf{d}_0 + \mathbf{D}\boldsymbol{\beta}. \quad (37)$$

This mixed-integer structure admits two fundamentally different algorithmic treatments, which we develop next.

We now derive an explicit QUBO formulation, including the closed-form expression of the QUBO matrix in Appendix A, using the binary variables defined as following.

**Binary encoding of continuous variables.** Let  $\mathbf{y} \in \mathbb{R}^{n_y}$  denote the continuous part of the decision vector. For each  $y_i \in [\ell_i, u_i]$ , we introduce  $K_y$  binary variables and write  $y_i = \ell_i + \sum_{k=1}^{K_y} t_k^{(y)} z_{ik}$ ,  $z_{ik} \in \{0, 1\}$ , where the bit weights  $t_k^{(y)}$  are chosen according to a target resolution (e.g.,  $t_k^{(y)} = 2^{k-1} \Delta_y$ ). Define the bit-weight vector

$$\mathbf{t}^{(y)} \triangleq [t_1^{(y)}, \dots, t_{K_y}^{(y)}]^\top \in \mathbb{R}^{K_y}.$$

and stack all bits as  $\mathbf{z}^{(y)} \in \{0, 1\}^{n_y K_y}$ . Then  $\mathbf{y} = \boldsymbol{\ell} + \mathbf{T}_y \mathbf{z}^{(y)}$ ,  $\mathbf{T}_y \triangleq \mathbf{I}_{n_y} \otimes (\mathbf{t}^{(y)})^\top \in \mathbb{R}^{n_y \times n_y K_y}$ , where  $\otimes$  denotes the Kronecker product.

**Slack variables for inequality constraints and their binary encoding.** Consider the inequality constraints

$$\mathbf{C}\mathbf{y} \leq \mathbf{d}_0 + \mathbf{D}\boldsymbol{\beta},$$

we introduce nonnegative slack variables  $\mathbf{s} \in \mathbb{R}_+^{m_c}$ , where  $m_c$  is the number of inequality constraints, and rewrite  $\mathbf{C}\mathbf{y} + \mathbf{s} = \mathbf{d}_0 + \mathbf{D}\boldsymbol{\beta}$ . To obtain a pure binary formulation, each slack component  $s_j \in [0, u_j^{(s)}]$  is encoded by  $K_s$  binary variables,  $s_j = \sum_{k=1}^{K_s} t_k^{(s)} w_{jk}$ , where  $w_{jk} \in \{0, 1\}$ . Let

$$\mathbf{t}^{(s)} \triangleq [t_1^{(s)}, \dots, t_{K_s}^{(s)}]^\top \in \mathbb{R}^{K_s}, \quad \mathbf{w} \in \{0, 1\}^{m_c K_s},$$

and define  $\mathbf{s} = \mathbf{T}_s \mathbf{w}$ , where  $\mathbf{T}_s \triangleq \mathbf{I}_{m_c} \otimes (\mathbf{t}^{(s)})^\top \in \mathbb{R}^{m_c \times m_c K_s}$ .

**Unified binary vector.** Collect all binary variables into a single vector

$$\mathbf{x} \triangleq [\mathbf{z}^{(y)}, \mathbf{w}, \boldsymbol{\beta}]^\top \in \{0, 1\}^{n_y K_y + m_c K_s + p}.$$

where  $p$  is the dimension of  $\boldsymbol{\beta}$ .

**Objective in terms of  $\mathbf{x}$ .** Recall that the objective is  $\tilde{\mathbf{c}}^\top \mathbf{y}$ , where  $\tilde{\mathbf{c}} = \mathbf{S}^\top \mathbf{c}$  and  $\mathbf{y} = \boldsymbol{\ell} + \mathbf{T}_y \mathbf{z}^{(y)}$ . Substituting yields

$$\tilde{\mathbf{c}}^\top \mathbf{y} = \tilde{\mathbf{c}}^\top \boldsymbol{\ell} + \tilde{\mathbf{c}}^\top \mathbf{T}_y \mathbf{z}^{(y)} = \text{const} + \begin{bmatrix} \mathbf{T}_y^\top \tilde{\mathbf{c}} \\ \mathbf{0} \\ \mathbf{0} \end{bmatrix}^\top \mathbf{x}.$$

This contributes a linear term in  $\mathbf{x}$  and a constant term independent of  $\mathbf{x}$ .

## Benders Decomposition for Structured Robustness Verification

An alternative, structurally more refined approach is to exploit the separability between  $\boldsymbol{\beta}$  and  $\mathbf{y}$  via Benders decomposition.

**Problem decomposition.** We treat  $\boldsymbol{\beta}$  as the complicating integer variables and  $\mathbf{y}$  as continuous variables. For any fixed  $\boldsymbol{\beta}$ , the resulting problem in  $\mathbf{y}$  is a linear program:

$$\text{SP}(\boldsymbol{\beta}) : \min_{\mathbf{y}} \tilde{\mathbf{c}}^\top \mathbf{y} \quad (38)$$

$$\text{s.t. } \mathbf{A}\mathbf{y} = \mathbf{b}_0 + \mathbf{B}\boldsymbol{\beta}, \quad (39)$$

$$\mathbf{C}\mathbf{y} \leq \mathbf{d}_0 + \mathbf{D}\boldsymbol{\beta}. \quad (40)$$

**Dual subproblem.** Let  $\boldsymbol{\pi}$  and  $\boldsymbol{\lambda} \geq 0$  denote the dual variables associated with the equality and inequality constraints, respectively. The dual reads:

$$\max_{\boldsymbol{\pi}, \boldsymbol{\lambda}} (\mathbf{b}_0 + \mathbf{B}\boldsymbol{\beta})^\top \boldsymbol{\pi} + (\mathbf{d}_0 + \mathbf{D}\boldsymbol{\beta})^\top \boldsymbol{\lambda} \quad (41)$$

$$\text{s.t. } \mathbf{A}^\top \boldsymbol{\pi} + \mathbf{C}^\top \boldsymbol{\lambda} = \tilde{\mathbf{c}}, \quad (42)$$

$$\boldsymbol{\lambda} \geq 0. \quad (43)$$

**Master problem.** Introduce a scalar variable  $\theta$  to represent the subproblem value. The Benders master problem is:

$$\min_{\boldsymbol{\beta}, \theta} \theta \quad (44)$$

$$\text{s.t. } \boldsymbol{\beta} \in \mathcal{B}, \quad (45)$$

$$\theta \geq \mathbf{b}_0^\top \boldsymbol{\pi}^k + \mathbf{d}_0^\top \boldsymbol{\lambda}^k + \boldsymbol{\beta}^\top (\mathbf{B}^\top \boldsymbol{\pi}^k + \mathbf{D}^\top \boldsymbol{\lambda}^k), \quad \forall k \in \mathcal{K}, \quad (46)$$

where each cut corresponds to an optimal dual solution  $(\boldsymbol{\pi}^k, \boldsymbol{\lambda}^k)$  of a previously solved subproblem, and  $\mathcal{B}$  encodes the integrality and logical constraints on  $\boldsymbol{\beta}$ , *i.e.*, if  $\text{SP}(\boldsymbol{\beta})$  is infeasible, a Farkas certificate  $(\hat{\boldsymbol{\pi}}, \hat{\boldsymbol{\lambda}})$  satisfying

$$\mathbf{A}^\top \hat{\boldsymbol{\pi}} + \mathbf{C}^\top \hat{\boldsymbol{\lambda}} = 0, \quad \hat{\boldsymbol{\lambda}} \geq 0$$

yields the feasibility cut

$$\mathbf{b}_0^\top \hat{\boldsymbol{\pi}} + \mathbf{d}_0^\top \hat{\boldsymbol{\lambda}} + \boldsymbol{\beta}^\top (\mathbf{B}^\top \hat{\boldsymbol{\pi}} + \mathbf{D}^\top \hat{\boldsymbol{\lambda}}) \leq 0.$$

**Algorithmic scheme.** The algorithm alternates between: (i) solving the master problem to obtain a candidate  $\boldsymbol{\beta}$ ; (ii) solving the subproblem  $\text{SP}(\boldsymbol{\beta})$ ; (iii) adding either an optimality or feasibility cut. Convergence is guaranteed in finitely many iterations since  $\boldsymbol{\beta}$  ranges over a finite set. This decomposition preserves exactness, avoids discretization of  $\mathbf{y}$ , and exposes a clear separation between combinatorial activation patterns and continuous verification geometry.

## Acknowledgement

The authors gratefully acknowledge the support from the National Natural Science Foundation of China through Grants Nos. 62461160263 and 62371050.

## Competing Interests

The authors declare no competing interests.

## References

- [1] Alex Krizhevsky, Ilya Sutskever, and Geoffrey E. Hinton. Imagenet classification with deep convolutional neural networks. In *Advances in Neural Information Processing Systems (NeurIPS)*, 2012.
- [2] Kaiming He, Xiangyu Zhang, Shaoqing Ren, and Jian Sun. Deep residual learning for image recognition. In *Proceedings of the IEEE Conference on Computer Vision and Pattern Recognition (CVPR)*, 2016.
- [3] Ashish Vaswani et al. Attention is all you need. In *Advances in Neural Information Processing Systems (NeurIPS)*, 2017.
- [4] Jacob Devlin, Ming-Wei Chang, Kenton Lee, and Kristina Toutanova. Bert: Pre-training of deep bidirectional transformers for language understanding. In *Proceedings of the 2019 conference of the North American chapter of the association for computational linguistics: human language technologies, volume 1 (long and short papers)*, pages 4171–4186, 2019.
- [5] Mariusz Bojarski, Davide Del Testa, Daniel Dworakowski, Bernhard Firner, Beat Flepp, Praseon Goyal, Lawrence D Jackel, Mathew Monfort, Urs Muller, Jiakai Zhang, et al. End to end learning for self-driving cars. *arXiv preprint arXiv:1604.07316*, 2016.
- [6] John Jumper, Richard Evans, Alexander Pritzel, Tim Green, Michael Figurnov, Olaf Ronneberger, Kathryn Tunyasuvunakool, Russ Bates, Augustin Žídek, Anna Potapenko, et al. Highly accurate protein structure prediction with alphafold. *nature*, 596(7873):583–589, 2021.
- [7] Kevin Eykholt, Ivan Evtimov, Earlene Fernandes, Bo Li, Amir Rahmati, Chaowei Xiao, Atul Prakash, Tadayoshi Kohno, and Dawn Song. Robust physical-world attacks on deep learning visual classification. In *Proceedings of the IEEE conference on computer vision and pattern recognition*, pages 1625–1634, 2018.
- [8] Christian Szegedy, Wojciech Zaremba, Ilya Sutskever, Joan Bruna, Dumitru Erhan, Ian Goodfellow, and Rob Fergus. Intriguing properties of neural networks. *arXiv preprint arXiv:1312.6199*, 2013.
- [9] Ian J Goodfellow, Jonathon Shlens, and Christian Szegedy. Explaining and harnessing adversarial examples. *arXiv preprint arXiv:1412.6572*, 2014.
- [10] Aleksander Madry, Aleksandar Makelov, Ludwig Schmidt, Dimitris Tsipras, and Adrian Vladu. Towards deep learning models resistant to adversarial attacks. In *International Conference on Learning Representations*, 2018.
- [11] Eric Wong and Zico Kolter. Provable defenses against adversarial examples via the convex outer adversarial polytope. In *International conference on machine learning*, pages 5286–5295. PMLR, 2018.
- [12] Jeremy Cohen, Elan Rosenfeld, and Zico Kolter. Certified adversarial robustness via randomized smoothing. In *international conference on machine learning*, pages 1310–1320. PMLR, 2019.
- [13] Guy Katz, Clark Barrett, David L Dill, Kyle Julian, and Mykel J Kochenderfer. Reluplex: An efficient smt solver for verifying deep neural networks. In *International conference on computer aided verification*, pages 97–117. Springer, 2017.
- [14] Vincent Tjeng, Kai Y Xiao, and Russ Tedrake. Evaluating robustness of neural networks with mixed integer programming. In *International Conference on Learning Representations 2019*.
- [15] Rudy R Bunel, Ilker Turkaslan, Philip Torr, Pushmeet Kohli, and Pawan K Mudigonda. A unified view of piecewise linear neural network verification. *Advances in neural information processing systems*, 31, 2018.

- [16] Shiqi Wang, Kexin Pei, Justin Whitehouse, Junfeng Yang, and Suman Jana. Efficient formal safety analysis of neural networks. *Advances in neural information processing systems*, 31, 2018.
- [17] Changliu Liu, Tomer Arnon, Christopher Lazarus, Christopher Strong, Clark Barrett, Mykel J Kochenderfer, et al. Algorithms for verifying deep neural networks. *Foundations and Trends® in Optimization*, 4(3-4):244–404, 2021.
- [18] Frank Arute, Kunal Arya, Ryan Babbush, Dave Bacon, Joseph C Bardin, Rami Barends, Rupak Biswas, Sergio Boixo, Fernando GSL Brandao, David A Buell, et al. Quantum supremacy using a programmable superconducting processor. *Nature*, 574(7779):505–510, 2019.
- [19] Andrew D King, Alberto Nocera, Marek M Rams, Jacek Dziarmaga, Roeland Wiersema, William Bernoudy, Jack Raymond, Nitin Kaushal, Niclas Heinsdorf, Richard Harris, et al. Beyond-classical computation in quantum simulation. *Science*, 388(6743):199–204, 2025.
- [20] Wenxin Li, Chuan Wang, Hai Wei, Shuai Hou, Chongyu Cao, Chengkang Pan, Yin Ma, and Kai Wen. Unified sparse optimization via quantum architectures and hybrid techniques. *Quantum Science and Technology*, 10(2):025059, 2025.
- [21] Wenxin Li, Chuan Wang, Hongdong Zhu, Qi Gao, Yin Ma, Hai Wei, and Kai Wen. Quantum-classical hybrid quantized neural network. *arXiv:2506.18240*.
- [22] Haoqi He, Yan Xiao, Wenzhi Xu, Ruoying Liu, Xiaokai Lin, and Kai Wen. Hiq-lip: A hierarchical quantum-classical method for global lipschitz constant estimation of relu networks. *arXiv:2503.16342*, 2025.
- [23] Xujie Song, Tong Liu, Shengbo Eben Li, Jingliang Duan, Wenxuan Wang, and Keqiang Li. Training multi-layer neural networks on ising machine. *arXiv:2311.03408*, 2023.
- [24] Nicola Franco, Tom Wollschläger, Nicholas Gao, Jeanette Miriam Lorenz, and Stephan Günemann. Quantum robustness verification: A hybrid quantum-classical neural network certification algorithm. In *2022 IEEE International Conference on Quantum Computing and Engineering (QCE)*, pages 142–153, 2022.
- [25] Ronald A Fisher. The use of multiple measurements in taxonomic problems. *Annals of eugenics*, 7(2):179–188, 1936.
- [26] Fabian Pedregosa, Gaël Varoquaux, Alexandre Gramfort, Vincent Michel, Bertrand Thirion, Olivier Grisel, Mathieu Blondel, Peter Prettenhofer, Ron Weiss, Vincent Dubourg, et al. Scikit-learn: Machine learning in python. *the Journal of machine Learning research*, 12:2825–2830, 2011.
- [27] Diederik P Kingma. Adam: A method for stochastic optimization. *arXiv preprint arXiv:1412.6980*, 2014.
- [28] Krishnamurthy Dvijotham, Robert Stanforth, Sven Gowal, Timothy A Mann, and Pushmeet Kohli. A dual approach to scalable verification of deep networks. In *UAI*, volume 1, page 3, 2018.
- [29] Alessio Lomuscio and Lalit Maganti. An approach to reachability analysis for feed-forward relu neural networks. *arXiv preprint arXiv:1706.07351*, 2017.
- [30] Souradeep Dutta, Susmit Jha, Sriram Sanakaranarayanan, and Ashish Tiwari. Output range analysis for deep neural networks. *arXiv preprint arXiv:1709.09130*, 2017.
- [31] Timon Gehr, Matthew Mirman, Dana Drachler-Cohen, Petar Tsankov, Swarat Chaudhuri, and Martin Vechev. Ai2: Safety and robustness certification of neural networks with abstract interpretation. In *2018 IEEE symposium on security and privacy (SP)*, pages 3–18. IEEE, 2018.
- [32] Xiaowei Huang, Marta Kwiatkowska, Sen Wang, and Min Wu. Safety verification of deep neural networks. In *International conference on computer aided verification*, pages 3–29. Springer, 2017.
- [33] Weiming Xiang, Hoang-Dung Tran, and Taylor T Johnson. Reachable set computation and safety verification for neural networks with relu activations. *arXiv preprint arXiv:1712.08163*, 2017.
- [34] Lily Weng, Huan Zhang, Hongge Chen, Zhao Song, Cho-Jui Hsieh, Luca Daniel, Duane Boning, and Inderjit Dhillon. Towards fast computation of certified robustness for relu networks. In *International Conference on Machine Learning*, pages 5276–5285. PMLR, 2018.

- [35] Weiming Xiang, Hoang-Dung Tran, and Taylor T Johnson. Output reachable set estimation and verification for multilayer neural networks. *IEEE transactions on neural networks and learning systems*, 29(11):5777–5783, 2018.
- [36] Shiqi Wang, Kexin Pei, Justin Whitehouse, Junfeng Yang, and Suman Jana. Formal security analysis of neural networks using symbolic intervals. In *27th USENIX Security Symposium (USENIX Security 18)*, pages 1599–1614, 2018.
- [37] Gurobi Optimization, LLC. Gurobi Optimizer Reference Manual, 2024.
- [38] Hai Wei et al. A versatile coherent ising computing platform. *Light: Science & Applications*, 15(1):74, 2026.
- [39] Osbert Bastani, Yani Ioannou, Leonidas Lampropoulos, Dimitrios Vytiniotis, Aditya Nori, and Antonio Criminisi. Measuring neural net robustness with constraints. *Advances in neural information processing systems*, 29, 2016.

## A Details of the QUBO formulation

**Equality system including slack variables.** The original equalities and the transformed inequalities read

$$\begin{aligned} \mathbf{A}\mathbf{y} &= \mathbf{b}_0 + \mathbf{B}\boldsymbol{\beta}, \\ \mathbf{C}\mathbf{y} + \mathbf{s} &= \mathbf{d}_0 + \mathbf{D}\boldsymbol{\beta}. \end{aligned}$$

Substituting the encodings for  $\mathbf{y}$  and  $\mathbf{s}$ ,

$$\begin{aligned} \mathbf{A}(\boldsymbol{\ell} + \mathbf{T}_y \mathbf{z}^{(y)}) &= \mathbf{b}_0 + \mathbf{B}\boldsymbol{\beta}, \\ \mathbf{C}(\boldsymbol{\ell} + \mathbf{T}_y \mathbf{z}^{(y)}) + \mathbf{T}_s \mathbf{w} &= \mathbf{d}_0 + \mathbf{D}\boldsymbol{\beta}. \end{aligned}$$

Equivalently,

$$\begin{aligned} \mathbf{A}\mathbf{T}_y \mathbf{z}^{(y)} - \mathbf{B}\boldsymbol{\beta} &= \mathbf{b}_0 - \mathbf{A}\boldsymbol{\ell}, \\ \mathbf{C}\mathbf{T}_y \mathbf{z}^{(y)} + \mathbf{T}_s \mathbf{w} - \mathbf{D}\boldsymbol{\beta} &= \mathbf{d}_0 - \mathbf{C}\boldsymbol{\ell}. \end{aligned}$$

Define the stacked right-hand side

$$\mathbf{r}_{\text{eq}} \triangleq \begin{bmatrix} \mathbf{b}_0 - \mathbf{A}\boldsymbol{\ell} \\ \mathbf{d}_0 - \mathbf{C}\boldsymbol{\ell} \end{bmatrix},$$

and the combined equality matrix

$$\mathbf{M}_{\text{eq}} \triangleq \begin{bmatrix} \mathbf{A}\mathbf{T}_y & \mathbf{0} & -\mathbf{B} \\ \mathbf{C}\mathbf{T}_y & \mathbf{T}_s & -\mathbf{D} \end{bmatrix}.$$

Then all constraints can be written compactly as  $\mathbf{M}_{\text{eq}}\mathbf{x} = \mathbf{r}_{\text{eq}}$ .

**Quadratic penalty and explicit QUBO.** We enforce the equalities via a quadratic penalty with parameter  $\rho > 0$ :

$$\frac{\rho}{2} \|\mathbf{M}_{\text{eq}}\mathbf{x} - \mathbf{r}_{\text{eq}}\|_2^2 = \frac{\rho}{2} \mathbf{x}^\top \mathbf{M}_{\text{eq}}^\top \mathbf{M}_{\text{eq}} \mathbf{x} - \rho \mathbf{r}_{\text{eq}}^\top \mathbf{M}_{\text{eq}} \mathbf{x} + \frac{\rho}{2} \|\mathbf{r}_{\text{eq}}\|_2^2.$$

Using the fact that  $\mathbf{T}_y = \mathbf{I}_{n_y} \otimes (\mathbf{t}^{(y)})^\top$ ,  $\mathbf{T}_s = \mathbf{I}_{m_c} \otimes (\mathbf{t}^{(s)})^\top$ , we have

$$\begin{aligned} \mathbf{A}\mathbf{T}_y &= \mathbf{A}(\mathbf{I}_{n_y} \otimes (\mathbf{t}^{(y)})^\top), \\ \mathbf{C}\mathbf{T}_y &= \mathbf{C}(\mathbf{I}_{n_y} \otimes (\mathbf{t}^{(y)})^\top), \\ \mathbf{T}_s &= \mathbf{I}_{m_c} \otimes (\mathbf{t}^{(s)})^\top. \end{aligned}$$

Partition  $\mathbf{x}$  as

$$\mathbf{x} = \begin{bmatrix} \mathbf{z}^{(y)} \\ \mathbf{w} \\ \boldsymbol{\beta} \end{bmatrix},$$

and write

$$M_{\text{eq}}^\top M_{\text{eq}} = \begin{bmatrix} Q_{yy} & Q_{ys} & Q_{y\beta} \\ Q_{sy} & Q_{ss} & Q_{s\beta} \\ Q_{\beta y} & Q_{\beta s} & Q_{\beta\beta} \end{bmatrix},$$

where the blocks are

$$\begin{aligned} Q_{yy} &= \mathbf{T}_y^\top (\mathbf{A}^\top \mathbf{A} + \mathbf{C}^\top \mathbf{C}) \mathbf{T}_y \\ &= (\mathbf{I}_{n_y} \otimes \mathbf{t}^{(y)}) (\mathbf{A}^\top \mathbf{A} + \mathbf{C}^\top \mathbf{C}) (\mathbf{I}_{n_y} \otimes (\mathbf{t}^{(y)})^\top), \\ Q_{ys} &= \mathbf{T}_y^\top \mathbf{C}^\top \mathbf{T}_s = (\mathbf{I}_{n_y} \otimes \mathbf{t}^{(y)}) \mathbf{C}^\top (\mathbf{I}_{m_c} \otimes (\mathbf{t}^{(s)})^\top), \\ Q_{y\beta} &= -\mathbf{T}_y^\top (\mathbf{A}^\top \mathbf{B} + \mathbf{C}^\top \mathbf{D}) = -(\mathbf{I}_{n_y} \otimes \mathbf{t}^{(y)}) (\mathbf{A}^\top \mathbf{B} + \mathbf{C}^\top \mathbf{D}), \\ Q_{ss} &= \mathbf{T}_s^\top \mathbf{T}_s = (\mathbf{I}_{m_c} \otimes \mathbf{t}^{(s)}) (\mathbf{I}_{m_c} \otimes (\mathbf{t}^{(s)})^\top), \\ Q_{s\beta} &= -\mathbf{T}_s^\top \mathbf{D} = -(\mathbf{I}_{m_c} \otimes \mathbf{t}^{(s)}) \mathbf{D}, \\ Q_{\beta\beta} &= \mathbf{B}^\top \mathbf{B} + \mathbf{D}^\top \mathbf{D}. \end{aligned}$$

The remaining blocks satisfy  $Q_{sy} = Q_{ys}^\top$ ,  $Q_{\beta y} = Q_{y\beta}^\top$ , and  $Q_{\beta s} = Q_{s\beta}^\top$ .

**Final QUBO matrix and linear term.** Collecting the original objective and the penalty term, the QUBO takes the standard form

$$\min_{\mathbf{x} \in \{0,1\}^{n_y K_y + m_c K_s + p}} \mathbf{x}^\top \mathbf{Q} \mathbf{x} + \mathbf{q}^\top \mathbf{x} + \text{const},$$

with

$$\mathbf{Q} = \frac{\rho}{2} M_{\text{eq}}^\top M_{\text{eq}},$$

and

$$\mathbf{q} = \begin{bmatrix} \mathbf{T}_y^\top \tilde{\mathbf{c}} \\ \mathbf{0} \\ \mathbf{0} \end{bmatrix} - \rho M_{\text{eq}}^\top \mathbf{r}_{\text{eq}}.$$

The structured blocks of  $\mathbf{Q}$  explicitly encode all pairwise interactions among the binary representations of  $\mathbf{y}$ , the slack variables  $\mathbf{s}$ , and the integer parameters  $\beta$ , yielding a QUBO formulation that is directly compatible with Ising-type hardware.

## B Proof of Theorem 2

*Proof.* Fix any  $\delta$  with  $\|\delta\|_p \leq \varepsilon$ . By definition,

$$f(\mathbf{x} + \delta) = g(\mathbf{x} + \delta) + \mathbf{r}(\mathbf{x} + \delta).$$

Apply (26) with  $\mathbf{a} = g(\mathbf{x} + \delta)$  and  $\mathbf{b} = \mathbf{r}(\mathbf{x} + \delta)$  to obtain

$$m(f(\mathbf{x} + \delta)) = m(g(\mathbf{x} + \delta) + \mathbf{r}(\mathbf{x} + \delta)) \geq m(g(\mathbf{x} + \delta)) - 2\|\mathbf{r}(\mathbf{x} + \delta)\|_\infty.$$

Using (25) yields  $m(f(\mathbf{x} + \delta)) \geq m(g(\mathbf{x} + \delta)) - 2\tau$ . Taking infimum over all feasible  $\delta$  gives the lower bound  $\Phi_f(\mathbf{x}; \varepsilon) \geq \Phi_g(\mathbf{x}; \varepsilon) - 2\tau$ . The upper bound follows identically from the upper inequality in (26). The statements involving  $L_g, U_g$  are immediate by substitution.  $\square$

## C Constructing the value of $\tau$

**Step 1: a compositional perturbation bound.** Define the layer maps

$$T_l(\mathbf{h}) := \sigma(\mathbf{W}_l \mathbf{h} + \mathbf{b}_l), \quad T_l'(\mathbf{h}) := \sigma'(\mathbf{W}_l \mathbf{h} + \mathbf{b}_l).$$

Let  $\|\cdot\|_{\infty \rightarrow \infty}$  denote the induced operator norm:  $\|\mathbf{A}\|_{\infty \rightarrow \infty} = \max_i \sum_j |A_{ij}|$ , *i.e.*, max absolute row-sum. Because  $\sigma$  is 1-Lipschitz in  $\|\cdot\|_{\infty}$ ,

$$\|T'_l(\mathbf{h}) - T'_l(\mathbf{h}')\|_{\infty} \leq \|\mathbf{W}'_l\|_{\infty \rightarrow \infty} \|\mathbf{h} - \mathbf{h}'\|_{\infty}. \quad (47)$$

Moreover, for the same input  $\mathbf{h}$ ,

$$\|T_l(\mathbf{h}) - T'_l(\mathbf{h})\|_{\infty} \leq \|(\mathbf{W}_l - \mathbf{W}'_l)\mathbf{h}\|_{\infty} = \|\Delta \mathbf{W}_l \mathbf{h}\|_{\infty} \leq \|\Delta \mathbf{W}_l\|_{\infty \rightarrow \infty} \|\mathbf{h}\|_{\infty}. \quad (48)$$

Now define the forward iterates for an input  $\mathbf{u}$ :  $\mathbf{h}_0(\mathbf{u}) = \mathbf{u}$ ,  $\mathbf{h}_l(\mathbf{u}) = T_l(\mathbf{h}_{l-1}(\mathbf{u}))$ ,  $\mathbf{h}'_l(\mathbf{u}) = T'_l(\mathbf{h}'_{l-1}(\mathbf{u}))$ . Set  $\mathbf{e}_l(\mathbf{u}) := \mathbf{h}_l(\mathbf{u}) - \mathbf{h}'_l(\mathbf{u})$ . Then

$$\mathbf{e}_l = T_l(\mathbf{h}_{l-1}) - T'_l(\mathbf{h}'_{l-1}) = \underbrace{(T_l(\mathbf{h}_{l-1}) - T'_l(\mathbf{h}_{l-1}))}_{\text{injected by pruning}} + \underbrace{(T'_l(\mathbf{h}_{l-1}) - T'_l(\mathbf{h}'_{l-1}))}_{\text{propagated error}}.$$

Taking  $\|\cdot\|_{\infty}$  and using (47)–(48),

$$\|\mathbf{e}_l(\mathbf{u})\|_{\infty} \leq \|\Delta \mathbf{W}_l\|_{\infty \rightarrow \infty} \|\mathbf{h}_{l-1}(\mathbf{u})\|_{\infty} + \|\mathbf{W}'_l\|_{\infty \rightarrow \infty} \|\mathbf{e}_{l-1}(\mathbf{u})\|_{\infty}. \quad (49)$$

Unrolling (49) from  $l = 1$  to  $L$  (with  $\mathbf{e}_0 = \mathbf{0}$ ) yields

$$\|\mathbf{h}_L(\mathbf{u}) - \mathbf{h}'_L(\mathbf{u})\|_{\infty} \leq \sum_{l=1}^L \left( \prod_{j=l+1}^L \|\mathbf{W}'_j\|_{\infty \rightarrow \infty} \right) \|\Delta \mathbf{W}_l\|_{\infty \rightarrow \infty} \|\mathbf{h}_{l-1}(\mathbf{u})\|_{\infty}. \quad (50)$$

If logits are  $\mathbf{z}_L$  rather than  $\mathbf{h}_L$ , the same argument applies with the last  $\sigma$  removed.

**Step 2: enforce uniformity over the perturbation ball.** To satisfy (25), we need bounds on intermediate activations in the adversarial ball. Assume we can compute (via IBP/CROWN/LP relaxations) constants  $H_{l-1}$  such that

$$\|\mathbf{h}_{l-1}(\mathbf{x} + \boldsymbol{\delta})\|_{\infty} \leq H_{l-1}, \quad \forall \|\boldsymbol{\delta}\|_p \leq \varepsilon.$$

Plugging into (50) gives the explicit computable bound

$$\tau \leq \sum_{l=1}^L \left( \prod_{j=l+1}^L \|\mathbf{W}'_j\|_{\infty \rightarrow \infty} \right) \|\Delta \mathbf{W}_l\|_{\infty \rightarrow \infty} H_{l-1}. \quad (51)$$